https://doi.org/10.5194/egusphere-2026-3417
Preprint. Discussion started: 29 July 2026

Uncertainty in computed turbulent heat fluxes over seasonal snow arising from roughness length and similarity theory assumptions

Katharina Theresa Scheidt[1,2], Rafael Pimentel[1], Paolo Deidda[2], Carlo Marin[2], Davide Gisolo[3], Davide Canone[3], María José Polo[1], Claudia Notarnicola[2], and Manuela Lehner[4]

[1]Fluvial Dynamics and Hydrology Research Group, Andalusian Institute for Earth System Research, University of Córdoba, Campus Rabanales, Edificio Leonardo da Vinci, 14014 Córdoba, Spain
[2]Institute for Earth Observation, Eurac Research, Viale Druso 1, 39100 Bolzano, Italy
[3]Interuniversity Department of Regional and Urban Studies and Planning (DIST), Politecnico and Università degli Studi di Torino, Viale Pier Andrea Mattioli 39, 10125 Torino, Italy
[4]Department of Atmospheric and Cryospheric Sciences, University of Innsbruck, Innrain 52f, 6020 Innsbruck, Austria

Correspondence: Katharina Theresa Scheidt (Katharina.Scheidt@eurac.edu)

Abstract. Aerodynamic roughness lengths are a key source of uncertainty in modeling turbulent heat fluxes over snow-covered surfaces, particularly in complex terrain. We investigate the influence of instrumental and measurement uncertainties and terrain complexity on roughness length estimates and MOST-based turbulent flux calculations using data from twelve eddy-covariance (EC) stations across the European Alps, covering slopes from $0.5°$ to $27.0°$. Two stations with multiple measurement levels allow for a detailed analysis of vertical wind profiles. Several bulk aerodynamic methods and roughness length parameterizations are evaluated.

Roughness lengths derived from logarithmic wind profiles under near-neutral conditions vary by up to an order of magnitude between measurement heights, indicating a strong sensitivity to sensor height and potential violations of the law of the wall. Instrumental and measurement uncertainties, especially under predominantly near-neutral or stable conditions with weak vertical gradients, lead to large relative errors in scalar roughness lengths and propagate into modeled turbulent fluxes, resulting in relative errors of up to $38.9\,\%$ for turbulent sensible heat flux and up to $56.5\,\%$ for turbulent latent heat flux.

Roughness lengths for momentum and scalars vary substantially among sites, and commonly assumed fixed ratios between them do not hold. No systematic degradation in bulk aerodynamic method performance with increasing slope is observed, suggesting that limitations arise from the general application of MOST in complex terrain. When EC-derived roughness lengths are unavailable, prescribing a constant roughness length ($0.61\,\mathrm{mm}$) for momentum and scalars provides the most robust EC-independent results.

1 Introduction

Mountains act as natural water towers storing water in the form of snow and ice during the winter months and releasing it as meltwater in spring and summer. This meltwater represents a crucial source of water for downstream ecosystems and human use (Barnett et al., 2005; Beniston et al., 2018). Accurately estimating water availability in downstream areas requires a sound understanding of the physical processes driving changes in the snowpack's energy and mass balance in upstream areas (Vano

https://doi.org/10.5194/egusphere-2026-3417
Preprint. Discussion started: 29 July 2026

et al., 2014). Among these processes, turbulent heat fluxes play a key role in the exchange of energy between the atmosphere and the snow or ice surface (Hock, 2005). These fluxes can substantially influence both snowmelt and evaposublimation. For example, periods of enhanced turbulent heat exchange have been linked to high melt rates (Braithwaite and Olesen, 1990; Hay and Fitzharris, 1988; Schlögl et al., 2018) and observations across various mountain regions have highlighted the significant contribution of evaposublimation to total snow ablation (Buri et al., 2023; Guo et al., 2021; Hanich et al., 2024; Hood et al., 1999; Litt et al., 2015; Lundquist et al., 2024; Stigter et al., 2018; Strasser et al., 2008; Voordendag et al., 2021).

Despite their importance, direct measurements of turbulent fluxes over snow and ice are relatively scarce, largely due to the limited availability of eddy-covariance (EC) towers, profile measurements, or lysimeter observations (Lundquist et al., 2024). This scarcity makes it challenging to understand the processes controlling turbulent exchange. In the absence of direct measurements, modelers typically rely on meteorological data from a single reference height and apply the bulk aerodynamic (BA) approach, assuming the validity of Monin–Obukhov Similarity Theory (MOST) to calculate turbulent heat fluxes between the snowpack and the atmosphere (Bartelt and Lehning, 2002; Essery, 2015; Herrero et al., 2009; Lehning et al., 2002; Strasser et al., 2024). The BA formulation further relies on the law of the wall (Von Kármán, 1931), which describes the logarithmic structure of mean wind profiles in the surface layer under neutral conditions and provides the theoretical basis for relating near-surface gradients to turbulent fluxes. However, this assumption is particularly problematic in complex mountain terrain, where the MOST–which assumes horizontal homogeneity and vertically constant fluxes–is often violated (Denby and Greuell, 2000; Radić et al., 2017; Schlögl et al., 2018).

Several sources of uncertainty arise when estimating turbulent heat fluxes using MOST. First, the assumption that two measurement levels–with the surface considered as one of them–are sufficient to reliably describe the logarithmic profiles of wind speed, temperature, and humidity introduces potential errors (Munro, 1989; Stiperski and Rotach, 2016). This assumption is valid for perfectly neutral stability conditions but is problematic under non-neutral conditions, where the actual profiles deviate from the ideal logarithmic form and require stability correction functions (Stull, 1988). Second, additional uncertainties originate from the estimation of surface conditions, especially surface temperature. For seasonal snow, surface temperature is difficult to determine accurately, as it is often not directly measured, and indirect estimates based on net longwave radiation are error-prone due to large measurement uncertainties that propagate into the calculated heat fluxes. In glacier studies, surface temperature is frequently assumed to be $0\,^{\circ}\mathrm{C}$ during summer melt periods (Hock, 2005; Radić et al., 2017). While this assumption is generally justified for melting glacier ice, it is more difficult to apply to seasonal snow. During winter, when snow temperatures typically remain below $0\,^{\circ}\mathrm{C}$, identifying melt periods–particularly given pronounced diurnal variability–can be challenging, making it difficult to confidently assume a surface temperature of $0\,^{\circ}\mathrm{C}$ or to constrain the surface temperature within an acceptable range of uncertainty. A third source of uncertainty arises from the specification of the roughness lengths for momentum ($z_{0\mathrm{v}}$), temperature ($z_{0\mathrm{T}}$), and humidity ($z_{0\mathrm{q}}$), which remain free, unknown parameters in the BA approach. However, obtaining reliable estimates of z_0 is not straightforward. Common approaches include aerodynamic methods, which derive (mean) values of $z_{0\mathrm{v}}$, $z_{0\mathrm{T}}$, and $z_{0\mathrm{q}}$ from profile or EC measurements, and geometrical methods, which relate $z_{0\mathrm{v}}$ to measurable surface characteristics of the snow cover, e.g., Brock et al. (2006).

https://doi.org/10.5194/egusphere-2026-3417
Preprint. Discussion started: 29 July 2026

Aerodynamic approaches are often limited by data availability, as only a small number of observations satisfy the requirements for stationarity and near-neutral conditions, which are rare over cold, snow- or ice-covered surfaces, where stable atmospheric stratification is typically observed (Radić et al., 2017; Fitzpatrick et al., 2019). Furthermore, over complex terrain, such as mountain regions, the validity of MOST is limited, since its underlying assumption of a flat and horizontally homogeneous surface is violated by topographic effects, e.g., katabatic flows that disturb the expected logarithmic wind profiles (Grachev et al., 2016; Radić et al., 2017). In addition, MOST is known to perform poorly in strongly stable boundary layers, where turbulence becomes intermittent, and similarity scaling breaks down–conditions that are common above snow- and ice-covered surfaces (Mahrt, 2014).

Geometrical approaches often rely on microtopographic measurements, for instance using digital photography to analyze individual snow surface profiles (Barella et al., 2026; Brock et al., 2006; Fassnacht et al., 2009a), or employing 3D reconstruction techniques such as LiDAR scanning (Fassnacht et al., 2023; Chambers et al., 2021; Smith et al., 2016) and Structure from Motion (SfM) photogrammetry (Liu et al., 2023; Smith et al., 2016). These geometrical methods follow the conceptual approach introduced by Lettau (1969), which relates surface roughness to the height, silhouette area and spacing of roughness elements. However, geometrical approaches, unless derived from airborne LiDAR measurements (Fassnacht et al., 2023), often fail to represent the influence of larger-scale topographic variability. Moreover, geometrical methods only provide estimates for $z_{0\mathrm{v}}$, whereas $z_{0\mathrm{T}}$ and $z_{0\mathrm{q}}$, which lack a direct physical meaning, remain undetermined.

Given these limitations and the general scarcity of reliable measurements, in most land-surface and snow models, a single effective roughness length is typically prescribed to represent the surface heterogeneity and complex terrain within the upwind fetch (Braithwaite, 1995; Martin and Lejeune, 1998). In the absence of direct roughness length measurements, z_0 is often subject to model calibration (e.g., Scheidt et al., 2025), or prescribed from literature values. The roughness lengths for temperature and humidity are then typically estimated using simplified relationships such as $z_{0\mathrm{T/q}} = z_{0\mathrm{v}}/100$ or $z_{0\mathrm{T/q}} = z_{0\mathrm{v}}$ (e.g. Essery, 2015; Hock and Holmgren, 2005; Hoffman et al., 2008; Sicart et al., 2005; Strasser et al., 2024), or surface renewal models (e.g., Andreas, 1987; Fitzpatrick et al., 2019; Smeets and Van den Broeke, 2008). While this simplification facilitates model application, it can introduce substantial uncertainty into the estimation of turbulent heat fluxes, and thus into simulated melt and sublimation rates. In addition, snow surface roughness is known to be site-specific and vary both spatially and temporally due to snow metamorphism, including changes to the snow surface due to wind redistribution, new snowfall, or the formation of snow cups during the melt period (Munro, 1989; Liu et al., 2023; Fassnacht et al., 2009b; Fassnacht, 2010; Fassnacht et al., 2023; Scheidt et al., 2025).

Taken together, these limitations indicate that uncertainty in turbulent heat flux estimates over seasonal snow arises not only from measurement error, but also from the assumptions used to retrieve and apply roughness lengths. Yet these sources of uncertainty are rarely assessed jointly across multiple snow-covered sites in complex terrain. To address this gap, we evaluate how measurement uncertainty, similarity-theory assumptions, and roughness length parameterizations affect estimates of surface roughness and turbulent heat fluxes over seasonal snow using observations from twelve EC stations across the European Alps.

https://doi.org/10.5194/egusphere-2026-3417
Preprint. Discussion started: 29 July 2026

Specifically, we (1) quantify how measurement uncertainties in wind speed and surface temperature propagate into roughness length and turbulent flux estimates; (2) evaluate how violations of MOST and the law of the wall affect roughness length retrievals; (3) compare roughness length variability across sites with different topographic and exposure conditions; and (4) assess how commonly used parameterizations of the BA method and roughness lengths $z_{0\mathrm{v}}$, $z_{0\mathrm{T}}$ and $z_{0\mathrm{q}}$ in snow models represent observed fluxes under these conditions.

We use EC observations from alpine grassland and pasture sites spanning a range of slopes and elevations, including both single- and multi-level installations. This dataset enables evaluation of MOST and the law of the wall under varying topographic and stability conditions. We compare bulk-aerodynamic formulations and roughness length parameterizations to quantify their sensitivity to measurement uncertainty and theoretical assumptions, and to identify where current approaches perform reliably and where improvements are needed.

This paper is organized as follows. In Section 2, a short background is given on the BA method, MOST and the derivation of roughness lengths. Section 3 describes the locations of the EC stations used in this study and outlines the applied pre- and postprocessing of the EC data (Subsections 3.1–3.3). Sections 3.6 and 3.7 briefly introduce the BA approaches and z_0 parameterizations employed. The analyses based on the law of the wall and the sensitivity analysis are presented in Sections 3.5 and 3.8, respectively. Finally, the results, discussion, and conclusions are given in Sections 4, 5, and 6.

https://doi.org/10.5194/egusphere-2026-3417
Preprint. Discussion started: 29 July 2026

105 **List of symbols**

Symbol	Meaning	Symbol	Meaning
u	Mean wind speed at measurement height z_u	u_*	Friction velocity
$\overline{u'w'}$, $\overline{v'w'}$	Turbulent momentum flux components	θ	Potential temperature at height z_T
θ_S	Surface potential temperature	θ_*	Temperature scaling parameter
T	Air temperature at height z_T	T_S	Snow surface temperature
q	Specific humidity at height z_q	q_S	Surface specific humidity, assumed saturated with respect to ice
q_*	Humidity scaling parameter	Q_H	Turbulent sensible heat flux
Q_L	Turbulent latent heat flux	ρ_a	Air density
c_p	Specific heat capacity of air at constant pressure	L_v	Latent heat of vaporization or sublimation
K_M	Eddy viscosity for momentum	K_H	Eddy diffusivity for heat
K_E	Eddy diffusivity for water vapor	Pr	Turbulent Prandtl number
k	von Kármán constant	g	Gravitational acceleration
L	Monin–Obukhov length	ζ	Stability parameter ($\zeta = z/L$)
Ψ_m	Stability correction function for momentum	Ψ_h	Stability correction function for heat and humidity
z_u	Wind measurement height above the snow surface	z_T	Temperature measurement height above the snow surface
z_q	Humidity measurement height above the snow surface	$z_\mathrm{T/q}$	Scalar measurement height
z_0v	Roughness length for momentum	z_0T	Roughness length for temperature
z_0q	Roughness length for humidity	$z_\mathrm{0T/q}$	Scalar roughness lengths for temperature and humidity
$z_\mathrm{0v,ec}$	Momentum roughness length derived from eddy-covariance data	$z_\mathrm{0T,ec}$	Temperature roughness length derived from eddy-covariance data
$z_\mathrm{0q,ec}$	Humidity roughness length derived from eddy-covariance data	C_θ	Bulk transfer coefficient for heat
C_q	Bulk transfer coefficient for humidity	C_log	Neutral bulk transfer coefficient based on logarithmic profiles
C_Rib	Bulk transfer coefficient using the bulk Richardson number	Ri_b	Bulk Richardson number
Φ	Atmospheric stability factor in the C_Rib method	R^*	Roughness Reynolds number
ν	Kinematic viscosity of air	h_S	Snow height
z'_i	Effective measurement height at level i above the snow surface	z_i	Instrument height at level i
u_i	Mean wind speed at measurement level i	u_{*i}	Friction velocity at measurement level i
m	Slope of the regression between u_i and u_{*i}	σ	Stefan–Boltzmann constant
ε_S	Snow emissivity	LW_in	Incoming longwave radiation
LW_out	Outgoing longwave radiation	P	Precipitation
ΔT	Temperature difference or temperature uncertainty, depending on context	Δq	Specific humidity uncertainty
Δz_u, $\Delta z_\mathrm{T/q}$	Uncertainty in effective measurement heights		

2 Theory

This section summarizes the theoretical basis of the bulk aerodynamic formulation and its link to Monin–Obukhov similarity theory, which together provide the framework for both estimating turbulent fluxes and deriving surface roughness lengths.

2.1 Bulk aerodynamic method

The bulk aerodynamic (BA) method is an approach typically used for estimating turbulent sensible and latent heat fluxes when meteorological parameters (temperature, wind speed, humidity, and pressure) are only available at a single measurement

https://doi.org/10.5194/egusphere-2026-3417
Preprint. Discussion started: 29 July 2026

height, and when information on friction velocity or surface-layer scaling parameters is not available–as is often the case in snowpack or glacier energy-balance modeling.

All BA methods used in this study originate from the gradient transport (or K-theory) formulation of turbulence (Stull, 1988), in which turbulent fluxes of heat and moisture are expressed as being proportional to the vertical gradients of potential temperature and specific humidity:

$$\overline{w'\theta'} = -u_*\theta_* = -K_H\frac{\partial\theta}{\partial z}, \qquad \overline{w'q'} = -u_*q_* = -K_E\frac{\partial q}{\partial z}, \tag{1}$$

with K_H and K_E the eddy diffusivities for heat and vapor exchange, which are related to the Prandtl number Pr and eddy viscosity K_M via $K_M = Pr\cdot K_H$ and $K_M = Pr\cdot K_E$ respectively.

According to the BA theory, we can describe the turbulent heat fluxes as an integrated form of Eq. 1 proportional to the finite difference in temperature and specific humidity at measurement height $z_{\mathrm{T/q}}$ and the surface:

$$Q_{\mathrm{H}} = \rho_{\mathrm{a}}c_{\mathrm{p}}C_\theta u(\theta-\theta_{\mathrm{S}}), \tag{2}$$

$$Q_{\mathrm{L}} = \rho_{\mathrm{a}}L_{\mathrm{v}}C_{\mathrm{q}}u(q-q_{\mathrm{S}}), \tag{3}$$

where L_{v} is the latent heat of vaporization ($2.514\,\mathrm{MJ\,kg^{-1}}$) or sublimation ($2.848\,\mathrm{MJ\,kg^{-1}}$) if $T_{\mathrm{S}}\leq 0\,^\circ\mathrm{C}$, $\overline{u}$ is the mean wind speed at height z_{u}, θ and θ_{S} are the mean values of potential temperature at height $z_{\mathrm{T/q}}$ and at the surface, q and q_{S} are the mean values of specific humidity at height $z_{\mathrm{T/q}}$ and at the surface, and $C_{\theta/q}$ are the bulk transfer coefficients of eddy diffusivity. The bulk transfer coefficients are derived from the logarithmic wind profile and are dependent on roughness lengths of momentum $z_{0\mathrm{v}}$, temperature $z_{0\mathrm{T}}$ and water vapor $z_{0\mathrm{q}}$.

2.2 Monin-Obukhov similarity theory and roughness lengths

The Monin-Obukhov similarity theory (MOST) provides a theoretical framework describing the structure of the atmospheric surface layer under conditions of mechanical and thermal turbulence. It relates turbulent fluxes to mean vertical gradients of wind speed, temperature, and humidity, and predicts that these profiles follow a logarithmic form modified by atmospheric stability (Eqs. 4-6). Within MOST, deviations from neutral stratification are expressed through stability correction functions, which depend on the Monin–Obukhov length L.

$$u = -\frac{u_*}{k}\left[\ln\left(\frac{z_{0\mathrm{v}}}{z_{\mathrm{u}}}\right)+\Psi_{\mathrm{m}}\left(\frac{z}{L}\right)\right], \tag{4}$$

$$T-T_{\mathrm{S}} = -\frac{\theta_*}{k}\left[\ln\left(\frac{z_{0\mathrm{T}}}{z_{\mathrm{T}}}\right)+\Psi_{\mathrm{h}}\left(\frac{z}{L}\right)\right], \tag{5}$$

$$q-q_{\mathrm{S}} = -\frac{q_*}{k}\left[\ln\left(\frac{z_{0\mathrm{q}}}{z_{\mathrm{q}}}\right)+\Psi_{\mathrm{h}}\left(\frac{z}{L}\right)\right]. \tag{6}$$

https://doi.org/10.5194/egusphere-2026-3417
Preprint. Discussion started: 29 July 2026

Here, $k = 0.41$ is the von Kármán constant, u_* is the friction velocity, and θ_* and q_* are the turbulent scaling parameters for temperature and specific humidity, respectively. The variables u, T, and q denote mean wind speed, air temperature, and specific humidity measured at heights z_u, z_T, and z_q above the (snow) surface. T_S and q_S represent the surface temperature and specific humidity, with q_S assumed to be saturated with respect to ice at T_S. The Monin–Obukhov length L is defined as:

$$L = \frac{\rho_\mathrm{a} c_\mathrm{p} u_*^3 T}{k g Q_\mathrm{H}}, \tag{7}$$

where ρ_a is air density, c_p is the specific heat capacity of air at constant pressure, g is gravitational acceleration, and Q_H is the turbulent sensible heat flux.

The functions Ψ_m and Ψ_h are stability correction functions that account for deviations from the logarithmic profiles of wind speed, temperature, and humidity under non-neutral atmospheric stratification. In this study, stability corrections for stable conditions follow (Beljaars and Holtslag, 1991), while for unstable conditions we adopt formulations consistent with the similarity functions of Dyer and Hicks (1970), expressed in their integrated form as:

$$\Psi_\mathrm{m}(\zeta) = \begin{cases} -\left(a\zeta + b\left(\zeta - \frac{c}{d}\right)e^{-d\zeta} + \frac{bc}{d}\right), & \text{if } \zeta > 0 \\ \ln\left(\left(\frac{1+y^2}{2}\right)\left(\frac{1+y}{2}\right)^2\right) - 2\arctan(y) + \frac{\pi}{2}, & \text{if } \zeta \leq 0 \end{cases} \tag{8}$$

$$\Psi_\mathrm{h}(\zeta) = \begin{cases} -\left(\left(1 + \frac{2}{3}a\zeta\right)^{1.5} + b\left(\zeta - \frac{c}{d}\right)e^{-d\zeta} + \frac{bc}{d} - 1\right), & \text{if } \zeta > 0 \\ 2\ln\left(\frac{1+y^2}{2}\right), & \text{if } \zeta \leq 0 \end{cases} \tag{9}$$

with $a = 1$, $b = 0.667$, $c = 5$, $d = 0.35$, $y = (1-16\zeta)^{1/4}$, and $\zeta = z_\mathrm{u}/L$ in Eq. 8 and $\zeta = z_\mathrm{T/q}/L$ in Eq. 9. The stability parameter ζ characterizes the stratification state of the atmospheric surface layer.

These stability correction functions ensure consistency between observed non-neutral profiles and the logarithmic structure predicted by MOST, thereby enabling robust estimation of roughness lengths from eddy-covariance measurements.

In this study, roughness lengths for momentum, temperature, and humidity (z_0v, z_0T, and z_0q) are derived using MOST, resulting in the following inverse relations:

$$z_\mathrm{0v} = z_\mathrm{u} \cdot \exp\left(-k \cdot \frac{u}{u_*} - \Psi_\mathrm{m}\left(\frac{z}{L}\right)\right), \tag{10}$$

$$z_\mathrm{0T} = z_\mathrm{T} \cdot \exp\left(-k \cdot \frac{T - T_\mathrm{S}}{\theta_*} - \Psi_\mathrm{h}\left(\frac{z}{L}\right)\right), \tag{11}$$

$$z_\mathrm{0q} = z_\mathrm{q} \cdot \exp\left(-k \cdot \frac{q - q_\mathrm{S}}{q_*} - \Psi_\mathrm{h}\left(\frac{z}{L}\right)\right). \tag{12}$$

https://doi.org/10.5194/egusphere-2026-3417
Preprint. Discussion started: 29 July 2026

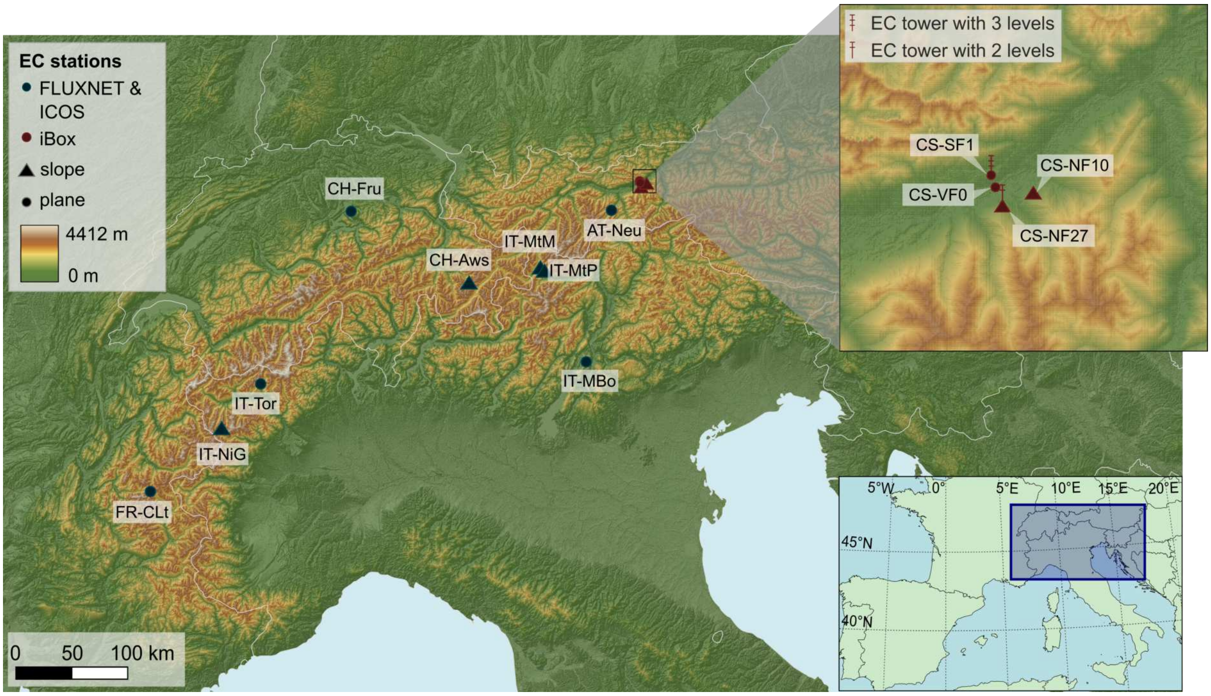

Figure 1. EC stations across the Alps. Stations located on a slope are visualized with a triangle, stations on flat surface with a circle. Dark blue symbols are linked to FLUXNET and ICOS stations and red symbols to i-Box stations. i-Box stations Kolsass (CS-SF1) and Hochhäuser (CS-NF27) are EC towers with three and two measurement levels, respectively.

3 Data and Methods

3.1 Eddy-covariance data

This study investigates the reliability of BA methods based on MOST in complex alpine terrain, considering variations in elevation, slope, and aspect. To this end, we analyzed data from twelve EC stations located across the European Alps (Table 1, Fig. 1). The sites are part of several established flux-monitoring networks, including FLUXNET (Pastorello et al., 2020), ICOS (Pastorello et al., 2020), the European Fluxes Database Cluster and the i-Box network operated by the University of Innsbruck (Rotach et al., 2017). From these datasets, we derived roughness lengths ($z_{0\mathrm{v}}$, $z_{0\mathrm{T}}$ and $z_{0\mathrm{q}}$) and used measured turbulent heat fluxes for evaluating the performance of BA approaches using the derived roughness lengths under diverse topographic conditions.

Stations were chosen based on several criteria. We focused on canopy-free environments, since trees and tall bushes introduce additional and difficult-to-quantify uncertainties related to displacement height and snow interception. Each site was required to include all variables necessary for estimating $z_{0\mathrm{v}}$, $z_{0\mathrm{T}}$ and $z_{0\mathrm{q}}$ as well as the corresponding turbulent heat fluxes. Although some alternative datasets extend further back in time, we restricted our analysis to 2012–2023 to match the availability of

https://doi.org/10.5194/egusphere-2026-3417
Preprint. Discussion started: 29 July 2026

the gap-filled Visible Infrared Imaging Radiometer Suite (VIIRS) snow cover fraction (SCF) product, which is available from January 2012. This ensured reliable identification of fully snow-covered periods and minimized potential contamination of the flux footprint by other land-cover types.

To investigate the influence of complex terrain on roughness length and turbulent heat flux estimates derived using the BA method, we analyzed data from EC stations located across diverse topographic settings. Seven stations were situated on predominantly flat terrain, either on plateaus (IT-MBo, IT-Tor, FR-CLt) or in valleys (AT-Neu, CH-Fru, CS-SF1, CS-VF0). In contrast, six stations were positioned on slopes ranging from 10.0 to 27.0° (CH-Aws, IT-MtP, IT-NiG, CS-NF27, CS-NF10). All EC stations, except i-Box Kolsass (CS-VF0) and i-Box Hochhäuser (CS-NF27), measured turbulent fluxes at a single height. At i-Box Kolsass, fluxes were measured using three sonic anemometers installed at heights of $4\,\mathrm{m}$, $8.68\,\mathrm{m}$, and $16.93\,\mathrm{m}$, and two open-path gas analyzers installed at $4\,\mathrm{m}$ and $16.93\,\mathrm{m}$, while at i-Box Hochhäuser, momentum flux was measured with two sonic anemometers at $1.5\,\mathrm{m}$ and $7.08\,\mathrm{m}$ and latent heat flux was measured with an open-path gas analyzer at $7.08\,\mathrm{m}$.

The analyzed datasets consist of half-hourly flux products already quality-controlled and publicly available through FLUXNET, ICOS, and i-Box. The FLUXNET, European Fluxes Database Cluster and ICOS data are processed using the standard FLUXNET2015 ONEFlux pipeline (Pastorello et al., 2020). For the calculation of roughness lengths and turbulent heat fluxes using the BA method, we used only the directly measured (non–gap-filled and non–energy-balance-corrected) data, as these represent the highest-quality observations. This choice ensures consistency across sites, as most stations lack snow temperature measurements, preventing reliable quantification of energy fluxes within the snowpack (e.g., melt) and thus precluding robust energy balance closure corrections.

The datasets of the i-Box stations were obtained from the online database of the Department of Atmospheric and Cryospheric Sciences of the University of Innsbruck (University of Innsbruck, ACInn, n.d.). In contrast to the data processed through the FLUXNET2015 ONEFlux pipeline, the i-Box datasets additionally include the turbulent fluxes $\overline{u'w'}$, $\overline{v'w'}$, $\overline{u'T'}$, $\overline{w'T'}$, and $\overline{w'q'}$, which enabled an assessment of flow regimes. For sites with multi-level measurements (i-Box Kolsass and i-Box Hochhäuser), this included the identification of characteristic flow patterns, such as valley winds at Kolsass and katabatic conditions at Hochhäuser. Radiative fluxes at the i-Box stations were provided as 1-min raw measurements. These data were manually filtered and quality-controlled and subsequently aggregated to half-hourly means to ensure consistency with the EC flux products.

3.2 Snow-Height Data

Snow-height data were used to identify periods with snow cover and to calculate the effective measurement heights of the sonic wind, temperature, and humidity sensors above the snow surface (z_u and $z_{\mathrm{T/q}}$). These heights were obtained as the difference between the instrument heights and the measured snow height. At several EC stations (AT-Neu, FR-CLt, IT-NiG, and IT-Tor), acoustic sensors continuously measured snow or vegetation height, providing snow-height data at 30-min resolution throughout the study period. At the remaining sites, snow height was either unavailable or only partially recorded. For these stations, snow-height data were obtained from nearby automatic weather stations (CH-Aws, CH-Fru, CS-SF1, CS-VF0, CS-NF27, CS-NF10, and IT-MtP) or from manual measurements (IT-MBo). Sonic snow-height measurements were corrected for sensor noise and

https://doi.org/10.5194/egusphere-2026-3417
Preprint. Discussion started: 29 July 2026

Table 1. EC station information including instrument heights for wind (z_u) and temperature (z_t). For i-Box stations with multiple measurement levels, values are given for all available levels.

Station name	Abbrev.	Elev. [m a.s.l.]	Lat / Lon [°N, °E]	Slope [°]	z_u [m]	z_t [m]	Years	EC dataset	Snow height source
Neustift	AT-Neu	970	47.116 / 11.320	1.2	2.50	2.50	2016–2020	Wohlfahrt (2024)	provided upon request
Alp Weissenstein	CH-Aws	1978	46.583 / 9.791	18.4	1.30	1.50	2012–2023	Buchmann et al. (2024)	MeteoSwiss
Früebüel	CH-Fru	982	47.116 / 8.538	0.8	2.55	1.80	2012–2023	Centre et al. (2019)	MeteoSwiss
Col du Lautaret	FR-CLt	2050	45.041 / 6.411	4.0	2.85	3.53	2022–2023	Voisin et al. (2024)	Voisin et al. (2024)
i-Box Eggen	CS-SF1	829	47.317 / 11.616	1.0	6.75	6.75	2017–2020	(University of Innsbruck, ACInn, n.d.)	HD
i-Box Kolsass	CS-VF0	545	47.305 / 11.622	0.5			2017–2020	(University of Innsbruck, ACInn, n.d.)	GeoSphere Austria
Level 1					4.00	4.00			
Level 2					8.68	–			
Level 3					16.93	16.93			
i-Box Hochhäuser	CS-NF27	1009	47.288 / 11.631	27.0			2017–2020	(University of Innsbruck, ACInn, n.d.)	GeoSphere Austria
Level 1					1.50	–			
Level 2					7.08	7.08			
i-Box Weerberg	CS-NF10	930	47.317 / 11.616	10.0	5.65	5.65	2017–2020	(University of Innsbruck, ACInn, n.d.)	GeoSphere Austria
Monte Bondone	IT-MBo	1550	46.015 / 11.046	3.6	2.37	2.37	2012–2021	Gianelle et al. (2022)	MeteoTrentino
							2022–2023	Gianelle et al. (2024)	
Muntatschinig Pasture	IT-MtP	1550	46.684 / 10.585	25.3	2.00	2.00	2017–2019	(Wohlfahrt and Niedrist, n.d.)	(Wohlfahrt and Niedrist, n.d.)
Nivolet	IT-NiG	2555	45.519 / 7.171	24.7	4.62	4.62	2021–2023	provided upon request	provided upon request
Torgnon	IT-Tor	2168	45.844 / 7.578	6.6	2.55	1.80	2016–2023	Cremonese et al. (2024)	Cremonese et al. (2024)

https://doi.org/10.5194/egusphere-2026-3417
Preprint. Discussion started: 29 July 2026

diurnal fluctuations related to sensor heating. Where only daily snow-height data were available (e.g., from local meteorological or hydrological services such as MeteoTrentino, MeteoSwiss, GeoSphere Austria, Hydrographischer Dienst Tirol, and SLF), these were linearly interpolated to the 30-min resolution of the EC data. This approach assumes gradual changes in snow surface height between observations and was considered sufficient for adjusting measurement heights rather than for analyzing short-term snow dynamics.

3.3 Snow surface temperature

The snow surface temperature T_S is required as a boundary condition in the bulk aerodynamic method and can be determined from net longwave radiation measurements available from the EC stations using the Stefan-Boltzmann law.

$$T_\mathrm{S} = \left[\frac{1}{\sigma\varepsilon_S}\left(LW_\mathrm{out} - (1-\varepsilon_S)LW_\mathrm{in}\right)\right]^{1/4}, \tag{13}$$

where σ is the Stefan–Boltzmann constant ($5.670 \times 10^{-8}\,\mathrm{W\,m^{-2}\,K^{-4}}$), and ε_S is the emissivity of snow, typically ranging from 0.97 to 0.995 (Dozier and Warren, 1982). Uncertainties in outgoing longwave radiation measured with a net radiometer can propagate into calculated surface-temperature errors of several Kelvin (Calanca, 2001; Radić et al., 2017). We therefore constrained the analysis primarily to snow-covered periods for which the snow surface was at the melting point. For each station, T_S was first calculated from longwave radiation using Eq. 13. Radiation-derived values exceeding $0\,^\circ\mathrm{C}$ were interpreted as non-physical for a snow surface and were capped at $T_\mathrm{S} = 0\,^\circ\mathrm{C}$. These periods were classified as melt-limited surface conditions.

As an additional consistency check, we evaluated the vertical snow-temperature profiles simulated by SNOWPACK (Bartelt and Lehning, 2002; Lehning et al., 1999, 2002) for these periods. Across stations, the majority of modeled profiles were near-isothermal, with vertical snow-temperature ranges below $0.2\,\mathrm{K}$ and temperatures close to the melting point, supporting the interpretation that the selected periods correspond to melt-limited snowpack conditions. However, because the SNOWPACK simulations are not fully independent of the prescribed surface-temperature forcing, they were used only as a consistency check and not as independent evidence of melt.

3.4 Determination of roughness length values obtained from EC stations

Roughness lengths of momentum, temperature and humidity (z_0v, z_0T and z_0q) were calculated by implementing EC data into the BA method using Eqs. 10-12.

To compute the roughness lengths z_0v, z_0T, and z_0q using Eqs. 10–12, one requires the friction velocity u_* and the temperature and humidity scaling parameters θ_* and q_*. For the i-Box datasets, the provided u_* was calculated as $u_* = \sqrt[4]{\overline{u'v'}^2 + \overline{v'w'}^2}$ accounting for the vertical contribution of $v'w'$ to the friction velocity on a slope site. For the ICOS and FLUXNET datasets, the friction velocity u_* was given in the datasets, while θ_* and q_* were obtained from the measured turbulent sensible and

https://doi.org/10.5194/egusphere-2026-3417
Preprint. Discussion started: 29 July 2026

latent heat fluxes, which can be parameterized as follows (Munro, 1989):

$$Q_{\mathrm{H}} = \rho_{\mathrm{a}}\, c_{\mathrm{p}}\, \theta_*\, u_*, \tag{14}$$

$$Q_{\mathrm{L}} = \rho_{\mathrm{a}}\, L_{\mathrm{v}}\, q_*\, u_*, \tag{15}$$

where L_{v} is the latent heat of vaporization ($2.514\,\mathrm{MJ\,kg^{-1}}$) or sublimation ($2.848\,\mathrm{MJ\,kg^{-1}}$) if $T_{\mathrm{S}} < 0\,°\mathrm{C}$.

When calculating $z_{0\mathrm{v}}$, $z_{0\mathrm{T}}$, and $z_{0\mathrm{q}}$, we focused on near-neutral atmospheric conditions ($|\zeta| \leq 0.1$), where turbulence is primarily generated by shear stress and thus closely linked to surface properties and the associated roughness lengths. Under these conditions, the influence of atmospheric stability correction functions is minimal. For nearly perfectly neutral cases ($|\zeta| \leq 0.01$), we assume that stability correction functions can be neglected entirely, allowing the expressions for $z_{0\mathrm{v}}$, $z_{0\mathrm{T}}$, and $z_{0\mathrm{q}}$ to simplify to the logarithmic forms:

$$z_{0\mathrm{v}} = z_{\mathrm{u}} \cdot \exp\left(-k \cdot \frac{u}{u_*}\right), \tag{16}$$

$$z_{0\mathrm{T}} = z_{\mathrm{T}} \cdot \exp\left(-k \cdot \frac{T - T_{\mathrm{S}}}{\theta_*}\right), \tag{17}$$

$$z_{0\mathrm{q}} = z_{\mathrm{q}} \cdot \exp\left(-k \cdot \frac{q - q_{\mathrm{S}}}{q_*}\right). \tag{18}$$

To ensure high-quality calculations of roughness lengths, we applied several quality control measures similar to Radić et al. (2017) and Fitzpatrick et al. (2019): (1) As indicated previously, we filtered for near-neutral atmospheric conditions (considering two cases: $|\zeta| \leq 0.1$ and $|\zeta| \leq 0.01$). (2) Furthermore, we only used flux data that passed the FLUXNET / ICOS quality control criteria, ensuring good overall data quality. These criteria include, among others, tests for stationarity, which ensure that turbulent fluxes were derived under quasi-steady conditions where the statistical properties of the flow remain constant over the 30-min averaging period. For the i-Box datasets, a separate quality flag indicating stationary fluxes was provided and used for filtering. (3) Low wind speeds or friction velocities often result in unrealistically large roughness lengths (on the order of meters) and introduce substantial uncertainty in their estimation. To mitigate this issue, we applied minimum thresholds for friction velocity ($u_{*\mathrm{min}} = 0.3\,\mathrm{m\,s^{-1}}$) and mean wind speed ($u_{\mathrm{min}} = 3\,\mathrm{m\,s^{-1}}$). (4) Since wind direction plays a critical role in determining $z_{0\mathrm{v}}$, we restricted our analysis to wind directions within a 90° window centered on the dominant wind direction during snow-covered periods. We also excluded data where wind flow distortion due to the station structure could be significant. (5) We further filtered out data points where wind speed surpassed a certain threshold for high probability of blowing snow events following Li and Pomeroy (1997) because advected particles entering the (open-path) gas analyzer can contaminate EC measurements. During such conditions the particles may interfere with the gas analyzer's optical path and alter gas concentration measurements (Heusinkveld et al., 2008). Furthermore, periods of blowing snow are not directly comparable to MOST, which does not account for the enhanced sublimation associated with the increased air–snow particle interface during blowing snow and hence tends to underestimate the turbulent fluxes (Sigmund et al., 2022). (6) A sufficient temperature difference between the snow surface and the measured air temperature ($\Delta T \geq 1\,\mathrm{K}$) was required, corresponding to a minimum water vapor pressure gradient of $66\,\mathrm{kPa}$ to ensure an adequate moisture gradient. (7) As net longwave radiation

https://doi.org/10.5194/egusphere-2026-3417
Preprint. Discussion started: 29 July 2026

measurements are often error-prone (Calanca, 2001; Radić et al., 2017), we only considered periods when the snowpack was melting, ensuring a surface temperature of $0\,°\mathrm{C}$. Periods of melting were identified as described in Section 3.3. (8) Periods with precipitation ($P > 0\,\mathrm{mm}$) were excluded due to potential contamination of open-path gas measurements (Fitzpatrick et al., 2017; Heusinkveld et al., 2008). (9) As mentioned earlier, we use SCF from VIIRS to distinguish between $z_{0\mathrm{v}}$, $z_{0\mathrm{T}}$ and $z_{0\mathrm{T}}$ calculated during fully snow-covered ($\mathrm{SCF} = 1$) and partially snow-covered ($\mathrm{SCF} < 1$) periods of times to determine the influence of other surface covers than snow within the flux footprint area. (10) Unrealistic values of roughness lengths were removed following the physical limits proposed by Andreas et al. (2010). Values of $z_{0\mathrm{T}}$ and $z_{0\mathrm{q}}$ smaller than 10^{-7} m were considered unphysical, as molecular diffusion cannot occur at smaller scales (Fitzpatrick et al., 2017). Values of $z_{0\mathrm{v}}$, $z_{0\mathrm{T}}$, or $z_{0\mathrm{q}}$ larger than $1\,\mathrm{m}$ were also discarded, as such high roughness lengths are physically implausible for snow-covered terrain and have not been observed (Brock et al., 2006). (11) For the i-Box Kolsass and i-Box Hochhäuser sites, where fluxes are measured at multiple heights and $\overline{u'w'}$ and $\overline{u'T'}$ are available, periods dominated by valley winds (i-Box Kolsass) or katabatic wind flow (i-Box Hochhäuser) could be identified and excluded from the analysis.

3.5 Evaluation of the law of the wall

The law of the wall, first described by Von Kármán (1931), states that under neutral atmospheric stratification the mean wind speed in turbulent flow increases logarithmically with distance from a solid boundary. In this study, we test the validity of the law of the wall in mountainous terrain and assess the influence of topography on the roughness length for momentum. This allows us to evaluate the reliability of roughness lengths derived from EC measurements at different installation heights in complex terrain.

To this end, data from two EC towers were analyzed. The i-Box Kolsass site is located in the Inn Valley on flat terrain (slope 0°) and is equipped with three sonic anemometers at three heights (Table 1). The i-Box Hochhäuser site is situated on a north-facing slope of 27° and features sonic anemometers at two heights.

To ensure the applicability of the logarithmic law, only periods with near-neutral atmospheric stability ($|\zeta| \leq 0.01$) were considered. Under these conditions, wind speed profiles are expected to collapse onto a pure logarithmic relationship if the law of the wall holds. The analysis was further restricted to periods with snow cover ($h_\mathrm{S} > 0\,\mathrm{m}$ and $\mathrm{SCF} > 0$). For both methods, $z_{0\mathrm{v}}$ was calculated separately for fully snow-covered conditions ($\mathrm{SCF} = 1$) and partially snow-covered conditions ($\mathrm{SCF} < 1$).

To increase the number of available data points, filters on surface temperature, which are applied in later parts of this study, were not used here, as the validity of the law of the wall is independent of surface temperature. However, low level wind-maxima as in katabatic wind conditions, which can disturb the logarithmic wind profile, were excluded. Specifically, cases were removed where $\overline{u'_1w'_1} > 0$ and $\overline{u'_2w'_2}$ (or $\overline{u'_3w'_3}$) < 0.

Three different methods were applied to derive the roughness length for momentum, $z_{0\mathrm{v}}$. In the first method, $z_{0\mathrm{v}}$ was calculated for each individual measurement level using the logarithmic wind profile under neutral conditions (Eq. 16). For each measurement level i, the friction velocity u_{*i} and the mean wind speed u_i were evaluated at the effective height above the snow surface, $z'_i = z_i - h_\mathrm{S}$, where z_i denotes the instrument height and h_S the snow height. The resulting $z_{0\mathrm{v}}$ values were then

https://doi.org/10.5194/egusphere-2026-3417
Preprint. Discussion started: 29 July 2026

compared between measurement levels. This method is also used in later parts of the study, as it can be applied at all stations equipped with only a single measurement level from a 3D sonic anemometer.

In the second method, $z_{0\mathrm{v}}$ was derived from the slope of a linear regression applied to scatterplots of u_i versus u_{*i}. Assuming the validity of the logarithmic wind profile, this regression slope can be related to the aerodynamic roughness length. The resulting slope m was used to infer $z_{0\mathrm{v}}$ by inverting the law-of-the-wall relationship,

$$z_{0\mathrm{v}} = z \cdot \exp(-k \cdot m),$$

where z is the measurement height. In this approach, temporal variations in snow height and roughness length are neglected. Consequently, the derived $z_{0\mathrm{v}}$ represents an effective mean value based on all available observations. Variations in snow height were not explicitly considered, since further binning of the dataset according to snow height would significantly reduce the number of remaining data points after filtering and thus limit statistical significance. Within the filtered dataset, maximum snow-height differences amount to 25 cm at i-Box Kolsass and 21 cm at i-Box Hochhäuser.

In the third method, a logarithmic wind profile was fitted to the mean wind speed measurements obtained from the two and three 3D sonic anemometers at i-Box Hochhäuser and i-Box Kolsass, respectively. The roughness length for momentum was treated as a fitting parameter. For comparison, the same analysis was conducted using four 2D sonic anemometers at i-Box Kolsass installed at heights of 2 m, 4 m, 6 m, and 12 m. This allowed us to compare momentum roughness lengths derived from wind profiles based on 2D sonic anemometers, 3D sonic anemometers, and a combined profile incorporating both instrument types at i-Box Kolsass.

3.6 Bulk aerodynamic methods

We tested two commonly used forms of heat transfer coefficients in snow modeling.

3.6.1 C_{log} method

The first form assumes a pure logarithmic wind speed profile in neutral atmospheric conditions, consequently discarding the atmospheric stability correction functions:

$$C_{\mathrm{log}} = \frac{k^2}{\ln\left(\frac{z_{\mathrm{u}}}{z_{0\mathrm{v}}}\right)\ln\left(\frac{z_{\mathrm{T/q}}}{z_{0T/q}}\right)}. \tag{19}$$

This parametrization is used in e.g. the WiMMed snow model, developed for the Sierra Nevada in Spain (Herrero et al., 2009).

3.6.2 C_{Rib} method

The second approach uses a formulation based on the bulk Richardson number Ri_{b}. This method is implemented in the snow models openAmundsen (Strasser et al., 2024) and FSM (Essery, 2015):

$$C_{Ri_{\mathrm{b}}} = \frac{k^2}{\ln\left(\frac{z_{\mathrm{u}}}{z_{0\mathrm{v}}}\right)\ln\left(\frac{z_{\mathrm{T/q}}}{z_{0T/q}}\right)}\Phi, \tag{20}$$

https://doi.org/10.5194/egusphere-2026-3417
Preprint. Discussion started: 29 July 2026

with Φ an atmospheric stability factor defined as:

$$\Phi(Ri_{\mathrm{b}}) = \begin{cases} \frac{1}{1+3b_{\mathrm{h}}Ri_{\mathrm{b}}(1+b_{\mathrm{h}}Ri_{\mathrm{b}})^{0.5}}, & \text{if } Ri_{\mathrm{b}} \geq 0 \\ \frac{1-3b_{\mathrm{h}}Ri_{\mathrm{b}}}{1+c(-Ri_{\mathrm{b}})^{0.5}}, & \text{if } Ri_{\mathrm{b}} < 0, \end{cases} \tag{21}$$

with the atmospheric stability parameter $b_{\mathrm{h}} = 5$ and the bulk Richardson number given by:

$$R_{\mathrm{ib}} = \frac{z_{\mathrm{u}}^2 g(T_z - T_{\mathrm{S}})}{z_{\mathrm{T/q}} T_z u^2}, \tag{22}$$

and

$$c = \frac{3b_{\mathrm{h}}^2 k^2 \left(\frac{z_{\mathrm{u}}}{z_{0\mathrm{v}}}\right)^{0.5}}{\left[\ln\left(\frac{z_{\mathrm{u}}}{z_{0\mathrm{v}}}\right)\right]^2}. \tag{23}$$

3.7 Roughness length parametrization

In addition to testing different BA methods, we explored five parameterizations of surface roughness lengths for scalars. The following formulations for $z_{0\mathrm{T}}$ and $z_{0\mathrm{q}}$ were evaluated.

The first parameterization derives roughness length of momentum, temperature, and humidity from Eqs. 10–12. The second parameterization prescribes $z_{0\mathrm{v}} = z_{0\mathrm{v,ec}}$ and $z_{0\mathrm{T/q}} = 0.1\, z_{0\mathrm{v,ec}}$. The third parameterization follows Essery (2015) and Strasser et al. (2024), with fixed values of $z_{0\mathrm{v}} = 0.01\,\mathrm{m}$ and $z_{0\mathrm{T}} = z_{0\mathrm{q}} = 0.1\, z_{0\mathrm{v}}$. The fourth parameterization assumes identical roughness lengths for momentum, temperature, and humidity $z_{0\mathrm{v}} = z_{0\mathrm{T}} = z_{0\mathrm{q}} = 0.61\,\mathrm{mm}$, consistent with the value used in Herrero and Polo (2016). The fifth parameterization is based on the surface renewal model proposed by Andreas (1987), which estimates the ratio of scalar to momentum roughness lengths as a function of the roughness Reynolds number:

$$\ln\left(\frac{z_{0T/q}}{z_{0\mathrm{v}}}\right) = b_0 + b_1 \ln(R^*) + b_2 \ln(R^*)^2, \tag{24}$$

where

$$R^* = \frac{u_* z_{0\mathrm{v}}}{\nu}, \tag{25}$$

ν is the kinematic viscosity of air ($1.5 \times 10^{-5}\,\mathrm{m^2\,s^{-1}}$), and b_0, b_1, and b_2 are empirical constants given in Andreas (1987) that vary with the flow regime (smooth, transitional, or rough). Although the original formulation of the Andreas model is, to our knowledge, not implemented in operational snow models, it offers a physically based approach for estimating scalar roughness lengths when $z_{0\mathrm{v}}$ is known (Fitzpatrick et al., 2019). We therefore include it here for evaluation.

An overview of all roughness length parameterizations considered in this study is given in Table 2.

3.8 Sensitivity analysis and error propagation

In this study, we assess the impact of instrumental and measurement uncertainties on the derived roughness lengths $z_{0\mathrm{v}}$, $z_{0\mathrm{T}}$, and $z_{0\mathrm{q}}$, and examine how these uncertainties propagate into turbulent heat fluxes calculated using the BA method. We

https://doi.org/10.5194/egusphere-2026-3417
Preprint. Discussion started: 29 July 2026

Table 2. Overview of roughness length parameterizations used in this study.

ID	$z_{0\mathrm{v}}$	$z_{0\mathrm{T}}$, $z_{0\mathrm{q}}$	Description
P1	$z_{0\mathrm{v,ec}}$	$z_{0\mathrm{T,ec}}$, $z_{0\mathrm{q,ec}}$	Derived from EC measurements (Eqs. 10–12)
P2	$z_{0\mathrm{v,ec}}$	$0.1\,z_{0\mathrm{v,ec}}$	Fixed ratio
P3	$0.01\,\mathrm{m}$	$0.1\,z_{0\mathrm{v}}$	Fixed values (Essery, 2015; Strasser et al., 2024)
P4	$0.61\,\mathrm{mm}$	$z_{0\mathrm{v}}$	Equal roughness lengths (Herrero and Polo, 2016)
P5	$z_{0\mathrm{v,ec}}$	Andreas (1987) model	Function of R^* (Andreas, 1987)

also assess how different combinations of BA methods and z_0 parameterizations perform across EC stations and how slope influences their performance.

In neutral conditions, uncertainties in $z_{0\mathrm{v}}$, $z_{0\mathrm{T}}$, and $z_{0\mathrm{q}}$ arise from uncertainties in the input variables u, u_*, z_u, $z_{\mathrm{T/q}}$, T, T_S, θ_*, q, q_S and q_*. All sources of uncertainty are accounted for, and the total propagated uncertainty is estimated using standard first-order error-propagation theory based on a Taylor series expansion.

For the turbulent scaling parameters, we assume relative uncertainties of $\Delta u_{*\mathrm{rel}} = \Delta\theta_{*\mathrm{rel}} = \Delta q_{*\mathrm{rel}} = 10\,\%$, reflecting the expected uncertainty of vertical fluxes for a constant flux layer (e.g., Dyer and Hicks, 1972). It should be noted, however, that this assumption relies on the presence of a well-defined constant-flux layer. Observational studies at i-Box stations suggest that this condition is often not fulfilled in complex terrain, where fluxes may vary considerably with height, leading to substantially larger effective uncertainties (e.g., Sfyri et al., 2018; Lehner et al., 2021). Accordingly, the adopted value should be interpreted as an optimistic estimate.

A relative uncertainty of $3\,\%$ is assigned to the mean wind speed u, which lies within the accuracy range specified by most sonic anemometer manufacturers.

Uncertainties in temperature and specific humidity are treated as uncertainties in the respective gradients $(T - T_\mathrm{S})$ and $(q - q_\mathrm{S})$. For temperature, the total uncertainty ΔT is composed of errors in both the measured air temperature T and the surface temperature T_S. Manufacturer specifications typically indicate an uncertainty of approximately $0.1\,\mathrm{K}$ for air temperature measurements. Given our filtering approach for T_S, we adopt an uncertainty of $\Delta T_\mathrm{S} = 0.2\,\mathrm{K}$.

For specific humidity, we follow the error estimates of Radić et al. (2017), who assume an uncertainty in water vapor pressure of $0.23\,\mathrm{hPa}$. This corresponds to an uncertainty in specific humidity of approximately $\Delta q \approx 1.6 \times 10^{-4}$.

Uncertainties in the measurement heights z_u and $z_{\mathrm{T/q}}$ are assumed to arise solely from uncertainties in snow height measurements, while the nominal instrument heights are treated as exact. For snow height measured directly at the EC station using a sonic ranger, we assume an uncertainty of $\Delta z_\mathrm{u} = \Delta z_{\mathrm{T/q}} = 2\,\mathrm{cm}$. This value is slightly more conservative than the nominal instrumental accuracy of typical ultrasonic snow-depth sensors (on the order of ~1 cm under ideal conditions), and is intended to account for additional sources of variability in field measurements, such as temperature-dependent changes in the speed of sound, sensor heating effects, and small-scale surface heterogeneity. For snow height estimates not obtained directly at the EC station, a larger and more conservative uncertainty of $\Delta z_\mathrm{u} = \Delta z_{\mathrm{T/q}} = 15\,\mathrm{cm}$ is applied, based on the maximum observed dif-

https://doi.org/10.5194/egusphere-2026-3417
Preprint. Discussion started: 29 July 2026

ference during overlapping measurement periods. This value is used as an upper-bound estimate in the absence of continuous co-located observations.

In a first step of the sensitivity analysis, relative errors in $z_{0\mathrm{v}}$, $z_{0\mathrm{T}}$, and $z_{0\mathrm{q}}$ were calculated for each individual data point based on the prescribed uncertainties. These relative errors were then averaged over all data points for each station.

In a second step, the uncertainties estimated for the roughness lengths were propagated into modeled turbulent sensible and latent heat fluxes using a Monte Carlo approach applied to the BA formulations described in Section 3.6. For this analysis, a less restrictive stability filter was used ($|\zeta| \leq 5$) to also include non-neutral conditions, under which the stability correction functions are non-zero. The analysis was further restricted to periods with complete snow cover ($\mathrm{SCF} = 1$).

We evaluated the two BA approaches introduced in Section 3.6 in combination with the five roughness length parameterizations described in Section 3.7 (Table 2).

For parameterizations P1 and P2, momentum and scalar roughness lengths were sampled from normal distributions defined by the mean roughness length values and their averaged relative uncertainties obtained from the first step of the sensitivity analysis based on Taylor error propagation. In addition, for all parameterizations, temperature, wind speed, and specific humidity gradients, as well as z_{u} and $z_{\mathrm{T/q}}$, were sampled from normal distributions. In each case, the observed value was used as the distribution mean and the corresponding prescribed uncertainty as the standard deviation, consistent with the uncertainty assumptions used in the roughness length error propagation.

4 Results

This section presents results on (i) the applicability of the law of the wall in complex terrain (Section 4.1), (ii) the propagation of instrumental and measurement uncertainties into roughness lengths and turbulent heat fluxes (Section 4.2), and (iii) the performance of different combinations of BA methods and z_0 parameterizations (Section 4.3). The comparison of BA formulations is restricted to the eight of the twelve stations for which sufficient data remained after applying all filtering criteria.

4.1 Law of the wall

To evaluate the validity of the law of the wall, momentum flux data from two EC towers in the Inn Valley were analyzed: i-Box Kolsass, located on flat terrain, and i-Box Hochhäuser, situated on a north-facing slope. Roughness lengths for momentum ($z_{0\mathrm{v}}$) were derived for near-neutral atmospheric conditions ($|\zeta| \leq 0.01$) during snow-covered periods using three different methods.

In the first approach, the logarithmic wind profile (Eq. 16) was applied directly to individual observations of mean wind speed u and friction velocity u_*, yielding time series of $z_{0\mathrm{v}}$ for each measurement level. Figures 2 a) and b) display the resulting roughness lengths for the three measurement heights at i-Box Kolsass and the two measurement heights at i-Box Hochhäuser, respectively.

At both sites, $z_{0\mathrm{v}}$ derived from different measurement levels exhibits substantial discrepancies, reaching differences of up to nearly two orders of magnitude for single data points. These discrepancies are generally smaller at i-Box Kolsass than at i-Box Hochhäuser. In particular, during December 2017, differences between the first ($z_{u,1} = 4.00\,\mathrm{m}$) and second ($z_{u,2} = 8.68\,\mathrm{m}$)

https://doi.org/10.5194/egusphere-2026-3417
Preprint. Discussion started: 29 July 2026

measurement levels at i-Box Kolsass are mostly negligible. In contrast, during February 2020, the maximum difference in $\log_{10}(z_{0v,i})$ between these two levels reaches approximately 0.8.

At i-Box Hochhäuser, differences in $\log_{10}(z_{0v,i})$ between the first and second measurement levels are consistently larger, typically ranging between 0.5 and 0.9. For both stations, the largest roughness lengths within a given time step are systematically obtained from the highest measurement level. This effect is more pronounced at the sloping i-Box Hochhäuser site.

In addition to differences between measurement levels, $z_{0\mathrm{v}}$ shows pronounced temporal variability. At i-Box Kolsass, for example, roughness lengths vary by approximately one order of magnitude within less than a day (11 December 2017, 09:00 to 11 December 2017, 21:00). During this period, $\log_{10}(z_{0v,1})$ and $\log_{10}(z_{0v,2})$ range from approximately -2 to -1, while $\log_{10}(z_{0v,3})$ varies from about -1.5 to -0.5.

The mean and standard deviation of $z_{0\mathrm{v}}$ were computed for each measurement level, along with the mean standard deviation between levels (Table 3). Roughness lengths derived during fully snow-covered conditions ($\mathrm{SCF} = 1$) and partially snow-covered periods ($\mathrm{SCF} < 1$) are generally comparable and fall within the same order of magnitude. However, the associated standard deviations indicate considerable variability.

Overall, the derived roughness lengths are consistent with values reported for old and rough snow and substantially exceed those typically observed over fresh snow, which generally lie in the (sub-)millimeter range (Brock et al., 2006).

To investigate whether the observed differences between measurement levels could be related to spatial heterogeneity in the contributing source areas, flux footprint climatologies were calculated for all measurement levels at i-Box Kolsass and i-Box Hochhäuser based on the datetimes included in the analysis above (Fig. 3).

At i-Box Kolsass, the footprints of all measurement levels predominantly cover agricultural land, with substantial overlap between levels. No systematic differences in land-cover type within the footprint areas are apparent between the different heights. Furthermore, differences in vegetation (e.g., grass and low crops) should be reduced even more for fully snow-covered periods ($\mathrm{SCF} = 1$).

At i-Box Hochhäuser, the footprints are more heterogeneous and show greater sensitivity to measurement height. While the lowest measurement level mainly samples grass-covered terrain, the footprint of the upper level partially extends towards forested areas. However, this forest contribution is limited to a small fraction of the total footprint area (within $80\,\%$ to $90\,\%$ cumulative contribution). Footprint differences may therefore contribute to the observed height dependence at Hochhäuser, but they do not appear sufficient to explain it fully.

The second approach estimated $z_{0\mathrm{v}}$ from a linear regression between mean horizontal wind speed u_i and friction velocity u_{*i} at each measurement level i using a robust Theil–Sen estimator (Fig. 4).

For i-Box Kolsass, the most consistent results across measurement levels were obtained for partially snow-covered conditions, with $z_{0\mathrm{v}}$ values ranging between $0.006\,\mathrm{m}$ and $0.024\,\mathrm{m}$. These values are comparable to the level-wise mean roughness lengths derived using the first method (Table 3). In contrast, all other cases yield substantially larger roughness lengths, typically on the order of $0.1\,\mathrm{m}$ at i-Box Kolsass (level 2, $\mathrm{SCF} = 1$) and reaching several meters at i-Box Hochhäuser (level 2, $\mathrm{SCF} < 1$).

https://doi.org/10.5194/egusphere-2026-3417
Preprint. Discussion started: 29 July 2026

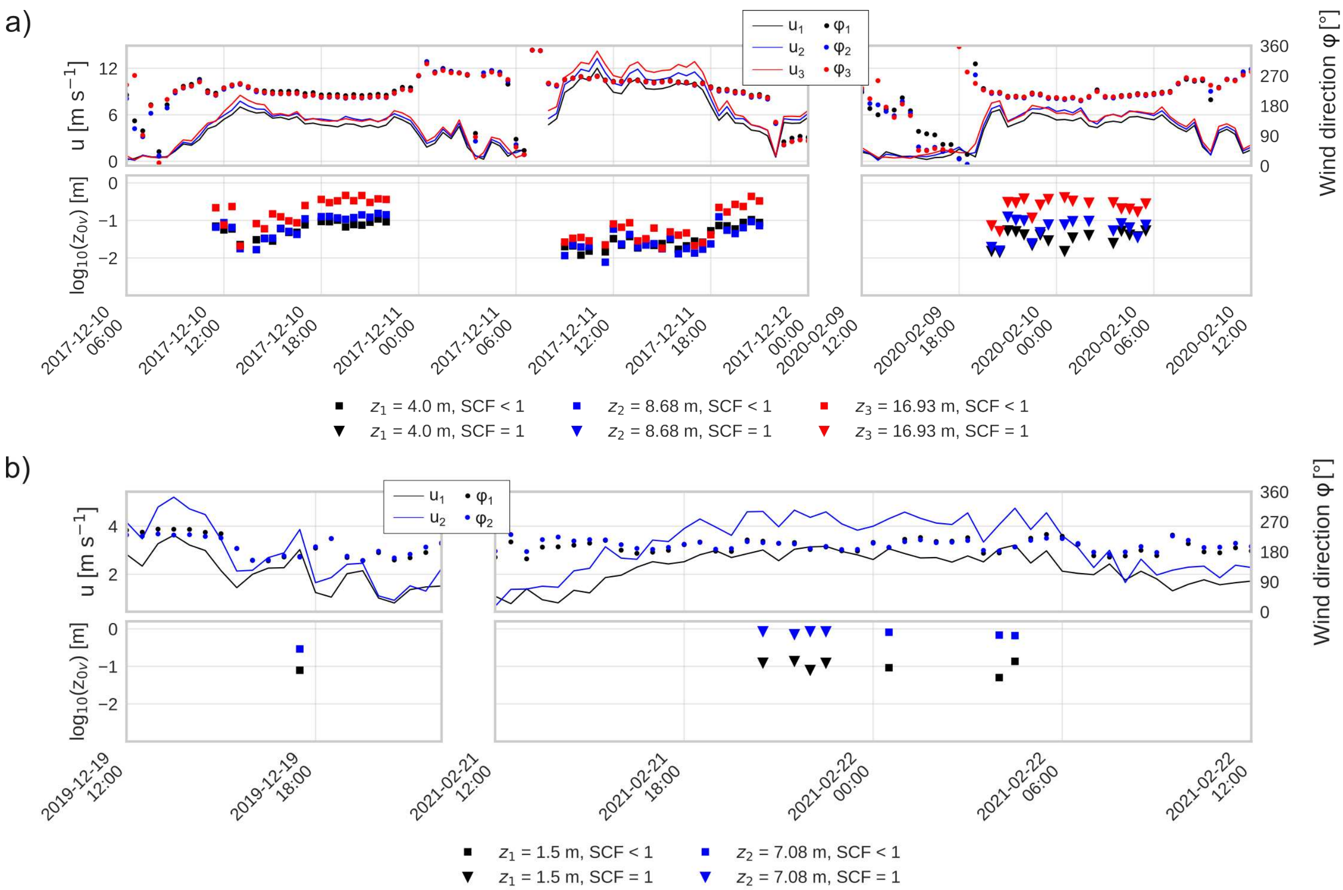

Figure 2. Roughness length of momentum $z_{0\mathrm{v}}$ for near-neutral atmospheric conditions calculated for the different measurement levels of mounted sonic anemometers at i-Box stations Kolsass (a) and Hochhäuser (b) using Eq. 16. The upper panels visualize wind speed and wind directions for all measurement levels. Dots in the $z_{0\mathrm{v}}$ plots represent periods of time with partial snow cover ($\mathrm{SCF} < 1$), triangles represent periods of time with full snow cover ($\mathrm{SCF} = 1$).

https://doi.org/10.5194/egusphere-2026-3417
Preprint. Discussion started: 29 July 2026

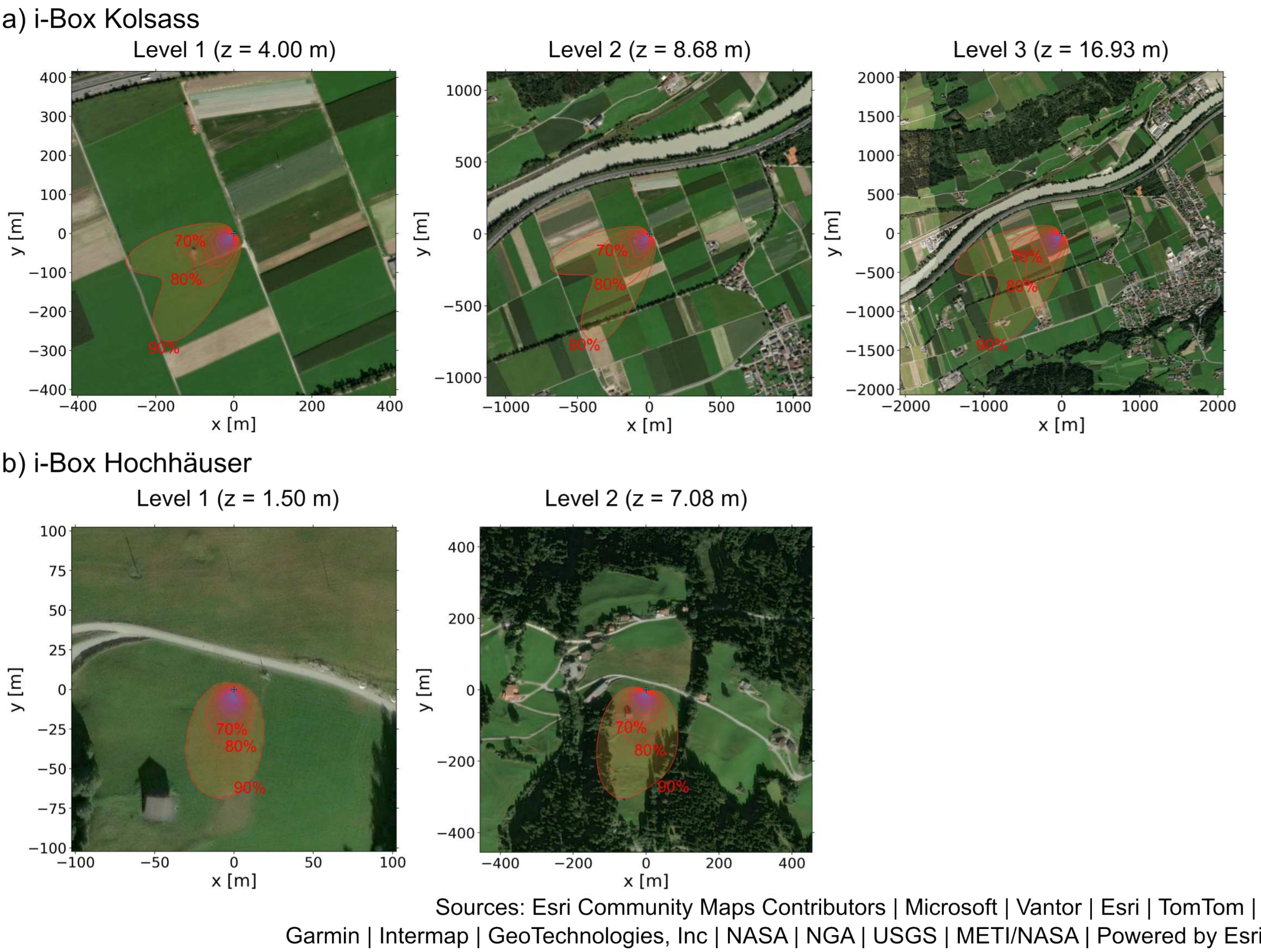

Figure 3. Flux footprint climatologies calculated using the FFPOnline tool provided by Kljun et al. (2015) for the filtered dataset used in the law-of-the-wall analysis. Shown are footprints for all three measurement levels at i-Box Kolsass (a) and for the two levels at i-Box Hochhäuser (b), based on wind directions with minimal tower-induced flow distortion. Orthophoto basemap from Esri World Imagery (Esri, 2026).

https://doi.org/10.5194/egusphere-2026-3417
Preprint. Discussion started: 29 July 2026

Table 3. Mean and standard deviation of aerodynamic roughness length (z_{0v}, in m) for different measurement heights at i-Box Kolsass and i-Box Hochhäuser. Two snow cover conditions are shown: full snow cover (SCF $= 1$) and partial snow cover (SCF < 1). $\overline{\sigma}$ denotes the mean of all σ_t values computed for each time step t across the measurement levels.

Site	**SCF**	$\overline{z_{0v,1}}$ [m]	$\sigma_{z_{0v,1}}$ [m]	$\overline{z_{0v,2}}$ [m]	$\sigma_{z_{0v,2}}$ [m]	$\overline{z_{0v,3}}$ [m]	$\sigma_{z_{0v,3}}$ [m]	$\overline{\sigma}$ [m]
i-Box Kolsass	SCF < 1	0.0513	0.0297	0.0589	0.0445	0.1610	0.1419	0.0628
	SCF $= 1$	0.0362	0.0143	0.0695	0.0334	0.2579	0.1093	0.1198
i-Box Hochhäuser	SCF < 1	0.0894	0.0358	0.6117	0.2240	–	–	0.3693
	SCF $= 1$	0.1188	0.0259	0.8358	0.0719	–	–	0.5070

These roughness lengths exceed values commonly reported in the literature for snow-covered surfaces by more than one order of magnitude (Brock et al., 2006). The large values are associated with substantial scatter in the u–u_* relationship and a limited number of available data points after filtering.

The third approach to deriving the momentum roughness length was based on fitting a logarithmic wind profile to mean wind speed measurements obtained from two or three vertical levels using 3D sonic anemometers, respectively. At i-Box Kolsass, additional mean wind speed measurements from four 2D sonic anemometers were included in the analysis. The resulting mean momentum roughness lengths are summarized in Table 4.

The mean momentum roughness length derived from fitting the logarithmic wind profile to the 3D sonic anemometer measurements at i-Box Hochhäuser was $0.0269\,\mathrm{m}$ during partially snow-covered periods and slightly higher, at $0.0576\,\mathrm{m}$, during fully snow-covered conditions. These values are of the same order of magnitude as the momentum roughness lengths derived from u_* and u at the first measurement level (Table 3), but are significantly smaller than those obtained from the second measurement level (Table 3 and Fig. 4(b)).

Momentum roughness lengths derived from logarithmic wind profiles using 3D and 2D sonic anemometer measurements at i-Box Kolsass ranged from sub-millimeter values for fully snow-covered periods when based on 3D profiles, to millimeter-scale values when based on 2D profiles. During partially snow-covered periods, momentum roughness lengths were approximately one order of magnitude larger, falling within the millimeter range for 3D profiles and the centimeter range for 2D profiles. A logarithmic fit to the combined wind speed profile derived from both 2D and 3D sonic anemometers was only feasible for partially snow-covered conditions, yielding a mean momentum roughness length of $0.0164\,\mathrm{m}$. Compared to the other two methods used to derive momentum roughness length, these values are generally smaller than those obtained using the linear regression and single-level approaches for fully snow-covered periods, while being of comparable magnitude to the regression-based estimates during partially snow-covered conditions.

Taken together, the three approaches show strong sensitivity of derived z_{0v} to retrieval method, measurement height, and instrument configuration. This sensitivity is evident at both sites and is more pronounced at the sloping Hochhäuser site.

https://doi.org/10.5194/egusphere-2026-3417
Preprint. Discussion started: 29 July 2026

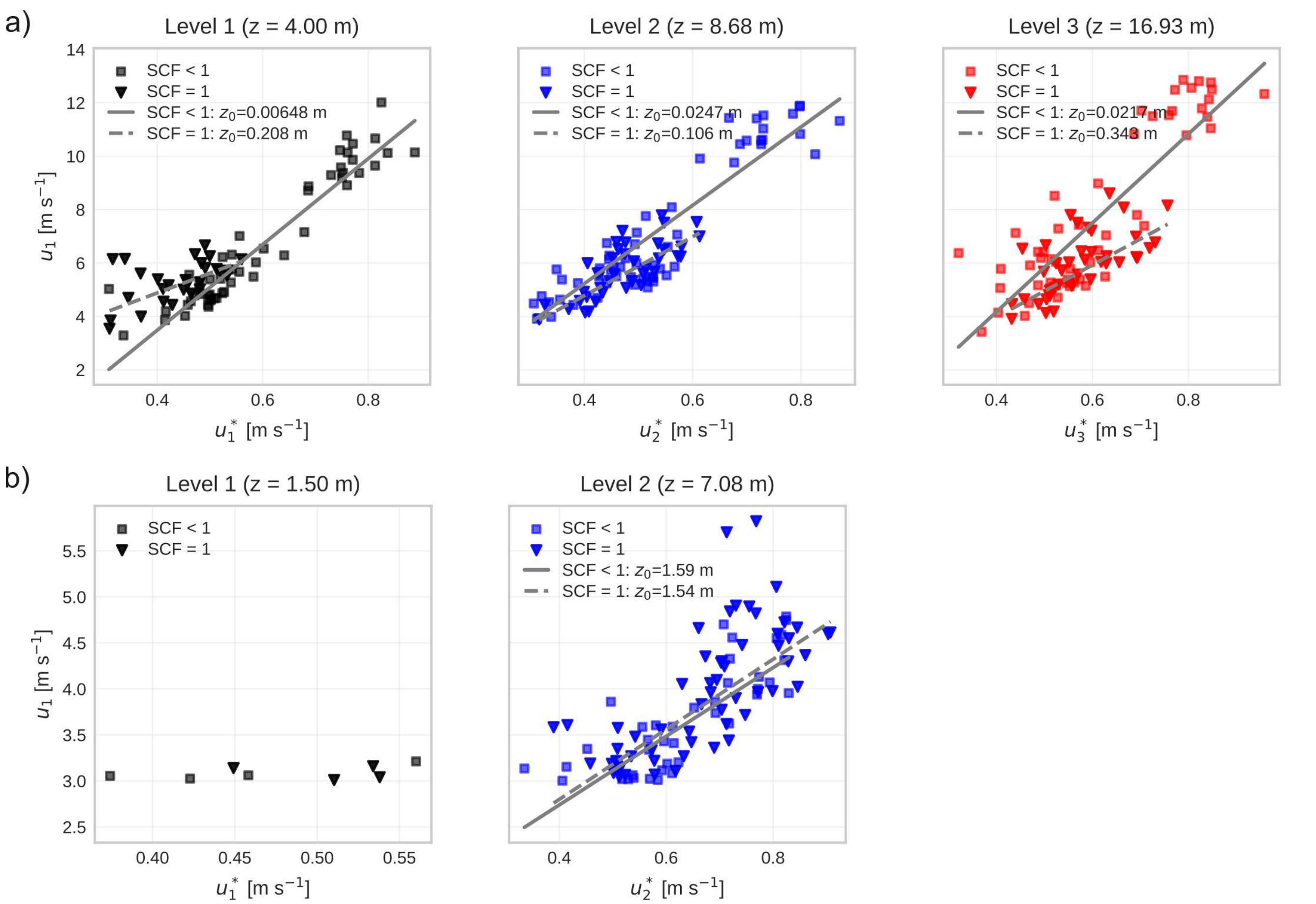

Figure 4. Roughness length for momentum z_{0v} at different measurement levels for i-Box Kolsass (a) and Hochhäuser (b). The values were calculated under near-neutral atmospheric conditions by fitting a linear regression (Theil–Sen method) between the mean horizontal wind speed u and the friction velocity u_*. Separate calculations were performed for periods of full snow cover ($\mathrm{SCF} = 1$, triangles) and partial snow cover ($\mathrm{SCF} < 1$, circles).

https://doi.org/10.5194/egusphere-2026-3417
Preprint. Discussion started: 29 July 2026

Table 4. Mean and standard deviation of aerodynamic roughness length ($z_{0\mathrm{v}}$, in m) computed using the profile method at i-Box Kolsass and i-Box Hochhäuser. For i-Box Kolsass, calculations were based on mean wind speeds from three 3D sonic anemometers and four 2D sonic anemometers. Two snow cover conditions are shown: full snow cover (SCF $=1$) and partial snow cover (SCF <1). $\overline{\sigma}$ represents the mean of the standard deviations across all profiles.

Site	**SCF**	$\overline{z_{0v,3D}}$ [m]	$\sigma_{z_{0v,3D}}$ [m]	$\overline{z_{0v,2D}}$ [m]	$\sigma_{z_{0v,2D}}$ [m]	$\overline{z_{0v,2D+3D}}$ [m]	$\sigma_{z_{0v,2D+3D}}$ [m]	$\overline{\sigma}$ [m]
i-Box Kolsass	SCF <1	0.0043	0.0047	0.0413	0.0181	0.0142	0.0164	0.0131
	SCF $=1$	0.0003	0.0003	0.0083	0.0058	–	–	0.0034
i-Box Hochhaeuser	SCF <1	0.0244	0.0208	–	–	–	–	0.0244
	SCF $=1$	0.0530	0.0236	–	–	–	–	0.0530

4.2 Error propagation

This sensitivity analysis examines how instrumental and measurement errors propagate into uncertainties in roughness lengths derived from EC data and how these uncertainties subsequently affect modeled turbulent heat fluxes in a Monte Carlo framework.

Table 5 summarizes mean roughness lengths and their averaged relative uncertainties for all sites under two stability criteria ($|\zeta| \leq 0.1$ and $|\zeta| \leq 0.01$). The relative uncertainties for individual data points are shown in Figures A1–A3. A first striking result is the strong reduction in available data under stricter stability filtering, particularly for scalar roughness lengths. For $|\zeta| \leq 0.1$, mean $z_{0\mathrm{T}}$ values are available for ten of the twelve stations, whereas mean $z_{0\mathrm{q}}$ values are available for only seven. Under the more restrictive criterion $|\zeta| \leq 0.01$, only one station provides estimates for both $z_{0\mathrm{T}}$ and $z_{0\mathrm{q}}$.

The mean momentum roughness lengths are similar across the two stability ranges. For $|\zeta| \leq 0.1$, $\log(z_{0\mathrm{v}})$ range from -1.89 to -0.19 (corresponding to $1.29-64.57\,\mathrm{cm}$), whereas for the more restrictive range $|\zeta| \leq 0.01$, the values span -1.78 to -0.25 (corresponding to $1.66-56.23\,\mathrm{cm}$). Across individual stations, $z_{0\mathrm{v}}$ values are generally consistent between the two stability conditions and of the same order of magnitude. Mean scalar roughness lengths ($z_{0\mathrm{T}}$ and $z_{0\mathrm{q}}$) are mostly substantially smaller than $z_{0\mathrm{v}}$, typically by one to three orders of magnitude, with the exception of Nivolet, where $\log(z_{0\mathrm{q}})$ with -0.99 is larger than $\log(z_{0\mathrm{v}})$ with -1.31. These scalar roughness lengths vary widely between stations. Furthermore, no clear relationship between $z_{0\mathrm{T}}$ and $z_{0\mathrm{q}}$ is observed; for a given station, the two quantities often differ by several orders of magnitude.

Regarding the relative uncertainties, momentum roughness length exhibits relative errors typically below $70\,\%$, whereas scalar roughness lengths show considerably larger uncertainties, frequently exceeding $100\,\%$. Temperature roughness length displays the highest uncertainties at most sites.

In the second step, these roughness length uncertainties were propagated into modeled turbulent sensible and latent heat fluxes using a Monte Carlo approach. Figures 5–8 show modeled versus measured fluxes for all retained stations, ordered by increasing slope angle, for all BA formulations and roughness length parameterizations introduced in Sections 3.6 and 3.7.

https://doi.org/10.5194/egusphere-2026-3417
Preprint. Discussion started: 29 July 2026

Table 5. Roughness length values in $\log(\mathrm{m})$ and their relative roughness length errors expressed in percent. Values are shown as mean (mean relative error) for two stability ranges. The number of available data points after filtering are indicated for each case (N_v, N_T and N_q). All roughness lengths are converted to $\log_{10}$ values.

Station	$\lvert\zeta\rvert \leq 0.1$						$\lvert\zeta\rvert \leq 0.01$					
	$\log_{10} z_{0\mathrm{v}}$ [m] ($\Delta z_{0\mathrm{v,rel}}$ [%])	N_v	$\log_{10} z_{0\mathrm{T}}$ [m] ($\Delta z_{0\mathrm{T,rel}}$ [%])	N_T	$\log_{10} z_{0\mathrm{q}}$ [m] ($\Delta z_{0\mathrm{q,rel}}$ [%])	N_q	$\log_{10} z_{0\mathrm{v}}$ [m] ($\Delta z_{0\mathrm{v,rel}}$ [%])	N_v	$\log_{10} z_{0\mathrm{T}}$ [m] ($\Delta z_{0\mathrm{T,rel}}$ [%])	N_T	$\log_{10} z_{0\mathrm{q}}$ [m] ($\Delta z_{0\mathrm{q,rel}}$ [%])	N_q
Monte Bondone	-0.86 (30.6)	136	-4.96 (131.1)	2	–	0	-0.80 (28.6)	66	–	0	–	0
Col du Lautaret	-1.75 (71.9)	664	-1.76 (102.3)	31	-3.26 (144.9)	15	-1.56 (66.9)	105	–	0	–	0
Torgnon	-1.50 (56.1)	966	-4.29 (192.4)	8	-3.70 (114.2)	7	-1.12 (40.6)	264	–	0	–	0
Neustift	-1.55 (55.1)	16	-5.26 (210.3)	16	-2.11 (70.8)	15	–	0	–	0	–	0
Alp Weissenstein	-1.89 (61.3)	923	-4.12 (213.5)	66	-4.33 (160.9)	32	-1.78 (58.8)	591	-4.02 (221.9)	39	-4.93 (156.9)	18
Mazia Pasture	-1.45 (45.7)	87	-5.65 (225.9)	6	-8.09 (217.9)	4	-1.56 (48.5)	18	–	0	–	0
Nivolet	-1.31 (56.7)	288	-2.53 (176.9)	8	-0.99 (98.3)	4	-1.26 (53.7)	74	–	0	–	0
i-Box Eggen	-0.67 (60.4)	117	–	0	–	0	-0.46 (34.7)	8	–	0	–	0
i-Box Hochhäuser												
Level 1	-0.93 (28.8)	4	–	0	–	0	–	0	–	0	–	0
Level 2	-0.19 (25.9)	61	-8.75 (395.8)	5	–	0	-0.25 (26.6)	1	–	0	–	0
i-Box Kolsass												
Level 1	-1.05 (57.8)	28	-4.31 (229.7)	7	-5.40 (190.3)	7	–	0	–	0	–	0
Level 2	-1.18 (56.4)	39	–	0	–	0	-1.06 (51.4)	2	–	0	–	0
Level 3	-0.56 (47.3)	41	-7.56 (345.7)	1	–	0	-0.40 (41.0)	1	–	0	–	0
i-Box Weerberg	-1.06 (50.0)	22	-2.12 (131.5)	5	–	0	–	0	–	0	–	0

https://doi.org/10.5194/egusphere-2026-3417
Preprint. Discussion started: 29 July 2026

Scatterplots are omitted where the number of observations remaining after quality control and stability filtering was insufficient for meaningful comparison, most notably for i-Box Kolsass level 3, i-Box Hochhäuser, i-Box Eggen, and Früebüel.

Vertical gray error bars indicate the propagated uncertainty in modeled turbulent fluxes arising from uncertainties in $z_{0\mathrm{v,ec}}$, $z_{0\mathrm{T,ec}}$, $z_{0\mathrm{q,ec}}$, temperature, wind speed, vapor pressure, and the turbulent scaling parameters u_*, θ_*, and q_*. Horizontal error bars represent the assumed $10\,\%$ uncertainty in the observed turbulent fluxes.

To summarize the magnitude of the propagated uncertainty in the modeled turbulent heat fluxes, we computed a relative Monte Carlo uncertainty metric,

$$\tilde{\sigma}_{\mathrm{rel,MC}} = \frac{\mathrm{median}(y_{\mathrm{err}})}{\mathrm{median}(|Q_{\mathrm{model}}|)},$$

where y_{err} denotes the vertical error bar obtained from the Monte Carlo propagation and Q_{model} the corresponding modeled turbulent flux. Thus, $\tilde{\sigma}_{\mathrm{rel,MC}}$ represents the typical propagated uncertainty relative to the typical magnitude of the modeled flux for a given station, BA formulation, and roughness length parameterization.

Using this metric, we generally find that the relative propagated uncertainty is larger for latent than for sensible heat flux. Across all investigated stations and parameterization combinations, $\tilde{\sigma}_{\mathrm{rel,MC}}$ reaches values of up to $38.9\,\%$ for Q_{H} (Col du Lautaret, P1) and up to $56.5\,\%$ for Q_{L} (Monte Bondone, P1).

Generally, the largest relative propagated uncertainties occur for the first roughness length parameterization (P1), in which Q_{H} and Q_{L} depend directly on the EC-derived roughness lengths $z_{0\mathrm{v,ec}}$, $z_{0\mathrm{T,ec}}$, and $z_{0\mathrm{q,ec}}$. For this parameterization, $\tilde{\sigma}_{\mathrm{rel,MC}}$ ranges from $19.7\,\%$ to $38.9\,\%$ for Q_{H} and from $22.7\,\%$ to $56.5\,\%$ for Q_{L} across the retained stations.

By contrast, propagated relative uncertainties are smaller for roughness length parameterizations that do not rely directly on EC-derived scalar roughness lengths. In these cases, the uncertainty in the modeled fluxes reflects only the prescribed uncertainties in meteorological input variables and turbulent scaling parameters.

Exceptionally high relative uncertainties are obtained at Monte Bondone for Q_{L} when using the P5 parameterization, exceeding $100\,\%$ for both BA formulations. However, this result is based on only three available data points, all associated with comparatively small modeled latent heat fluxes. The large relative uncertainties therefore mainly reflect the small flux magnitude and limited sample size rather than a generally poor performance of P5 at this site.

4.3 Comparison of BA formulations and z_0 parameterizations

This section compares the performance of different BA formulations combined with multiple roughness length parameterizations. Modeled turbulent sensible and latent heat fluxes are evaluated against EC measurements using RMSE, MBE, and Pearson r, as illustrated in the scatterplots in Figures 5–8 and Fig. 9.

At first glance, comparison of scatterplots across different BA formulations and z_0 parameterizations does not reveal a single parameterization that clearly outperforms the others. One exception is the first z_0 parameterization using $z_{0\mathrm{v,ec}}$, $z_{0\mathrm{T,ec}}$, and $z_{0\mathrm{q,ec}}$ in combination with the $C_{\log}$ formulation, which generally shows good agreement with the measured fluxes across stations and stability regimes. This is expected, as the $C_{\log}$ formulation effectively inverts roughness lengths that were themselves derived from the observed fluxes. Nevertheless, small deviations are evident, even under near-neutral

https://doi.org/10.5194/egusphere-2026-3417
Preprint. Discussion started: 29 July 2026

conditions. The most pronounced discrepancies thereby occur for latent heat fluxes under unstable conditions at the Nivolet station (RMSE $= 13.7\,\mathrm{W\,m^{-2}}$) and for sensible heat fluxes under predominantly near-neutral conditions at the Neustift station (RMSE $= 15.8\,\mathrm{W\,m^{-2}}$). Moreover, during stable conditions (blue), turbulent fluxes computed with C_{log} generally agree better with the measurements than those under near-neutral conditions, for which latent heat fluxes are mostly slightly underestimated and sensible heat fluxes slightly overestimated.

To compare the overall performance of the different BA–z_0 combinations more systematically, we ranked each combination for each station and level using RMSE, absolute bias ($|\mathrm{MBE}|$), and Pearson r (Table 6). Station-level ranks were averaged with equal weighting and then aggregated across all stations using the median. This ranking confirms that P1 combined with C_{log} performs best overall for both Q_{H} and Q_{L}.

In contrast, the C_{Rib} formulation combined with P1 exhibits a larger spread of data points and overall slightly poorer agreement with the measurements. Modeled sensible heat fluxes consistently show a positive bias, whereas modeled latent heat fluxes exhibit a negative bias across stations. The largest discrepancies are again observed at the Neustift station, where the RMSE reaches $54.7\,\mathrm{W\,m^{-2}}$. Another notable exception is observed at the Nivolet station, where sensible heat fluxes are consistently underestimated for the unstable regime across both BA formulations and all z_0 parameterizations, excluding those based directly on EC-derived roughness lengths.

Among the parameterizations independent of EC-derived scalar roughness lengths, the poorest performance is obtained for P2 with C_{log}, i.e. EC-derived $z_{0\mathrm{v}}$ combined with the fixed ratio $z_{0\mathrm{T/q}} = 0.1\,z_{0\mathrm{v,ec}}$. This combination ranks last for Q_{L} and also performs poorly for Q_{H}, with RMSE frequently exceeding $50\,\mathrm{W\,m^{-2}}$ and reaching $155.0\,\mathrm{W\,m^{-2}}$ at Neustift. Poor performance is also observed for P3 (triangles, pointing to top), which prescribes $z_{0\mathrm{v}} = 0.01\,\mathrm{m}$ and $z_{0\mathrm{T/q}} = 0.1\,z_{0\mathrm{v}}$, particularly for sensible heat flux. Both parameterizations tend to produce a negative bias in Q_{H} across most stations.

The best agreement between modeled and measured fluxes–aside from the first parameterization at most stations–is achieved using the Andreas model (P5, visualized as diamonds in Fig. 9 and Table 6). However, the number of available data points is often reduced (see Fig. 9 (f)–(g)), because the computation of $z_{0\mathrm{T}}$ and $z_{0\mathrm{q}}$ frequently fails due to physically or mathematically invalid values.

Among the simpler fixed parameterizations, the assumption of equal roughness lengths for momentum, temperature, and humidity ($z_{0\mathrm{v}} = z_{0\mathrm{T}} = z_{0\mathrm{q}} = 0.61\,\mathrm{mm}$, P4, visualized as down pointing triangles) provides the most consistent agreement with observations.

Some station-specific exceptions remain. At Nivolet, sensible heat flux is consistently underestimated under unstable conditions across both BA formulations and nearly all z_0 parameterizations except those based directly on EC-derived roughness lengths. At Neustift, several BA–z_0 combinations show particularly large RMSE and bias values compared with the other stations.

One objective of this analysis was to assess whether the performance of BA methods and z_0 parameterizations systematically degrades with increasing terrain slope. Figure 9 shows RMSE, MBE, and Pearson r for each combination of roughness length parameterization and BA formulation across stations ordered by slope. A substantial variability in model performance is observed across stations. For sensible heat flux, RMSE ranges from $4.9\,\mathrm{W\,m^{-2}}$ (Monte Bondone, P1–C_{log}) to $155.0\,\mathrm{W\,m^{-2}}$

https://doi.org/10.5194/egusphere-2026-3417
Preprint. Discussion started: 29 July 2026

Table 6. Ranking of BA formulations and roughness length (z_0) parameterizations for sensible (Q_H) and latent (Q_L) heat fluxes. Rankings are based on station-wise ranks of Pearson correlation (r), RMSE, and absolute mean bias ($|\mathrm{MBE}|$), combined with equal weighting. Median scores and interquartile ranges (IQR) summarize performance across stations. Lower scores indicate better performance. Symbols represent each BA–z_0 combination and are consistent with those shown in Fig. 9.

Flux	z_0 parameterization	C-method	Symbol	Median	IQR	Rank
Q_H	$z_{0\mathrm{v,ec}}$, $z_{0\mathrm{T/q,ec}}$ (P1)	C_{log}	●	4.0	1.0	1
	$z_{0\mathrm{v,ec}}$, $z_{0\mathrm{T/q,Andreas}}$ (P5)	C_{log}	◆	9.5	7.0	2
	$z_{0\mathrm{v}} = z_{0\mathrm{T/q}} = 0.61\,\mathrm{mm}$ (P4)	C_{log}	▼	14.0	4.0	3
	$z_{0\mathrm{v,ec}}$, $z_{0\mathrm{T/q,ec}}$ (P1)	$C_{\mathrm{Ri_b}}$	○	14.0	4.0	3
	$z_{0\mathrm{v,ec}}$, $z_{0\mathrm{T/q,Andreas}}$ (P5)	$C_{\mathrm{Ri_b}}$	◇	14.0	6.8	3
	$z_{0\mathrm{v}} = 0.01\,\mathrm{m}$, $z_{0\mathrm{T/q}} = 0.1\,z_{0\mathrm{v}}$ (P3)	$C_{\mathrm{Ri_b}}$	△	19.0	2.0	4
	$z_{0\mathrm{v}} = z_{0\mathrm{T/q}} = 0.61\,\mathrm{mm}$ (P4)	$C_{\mathrm{Ri_b}}$	▽	20.0	2.0	5
	$z_{0\mathrm{v,ec}}$, $z_{0\mathrm{T/q}} = 0.1\,z_{0\mathrm{v,ec}}$ (P2)	$C_{\mathrm{Ri_b}}$	□	20.0	6.0	5
	$z_{0\mathrm{v}} = 0.01\,\mathrm{m}$, $z_{0\mathrm{T/q}} = 0.1\,z_{0\mathrm{v}}$ (P3)	C_{log}	▲	24.0	7.0	6
	$z_{0\mathrm{v,ec}}$, $z_{0\mathrm{T/q}} = 0.1\,z_{0\mathrm{v,ec}}$ (P2)	C_{log}	■	26.0	3.0	7
Q_L	$z_{0\mathrm{v,ec}}$, $z_{0\mathrm{T/q,ec}}$ (P1)	C_{log}	●	4.0	0.5	1
	$z_{0\mathrm{v,ec}}$, $z_{0\mathrm{T/q,ec}}$ (P1)	$C_{\mathrm{Ri_b}}$	○	9.5	2.5	2
	$z_{0\mathrm{v,ec}}$, $z_{0\mathrm{T/q,Andreas}}$ (P5)	C_{log}	◆	10.5	8.3	3
	$z_{0\mathrm{v,ec}}$, $z_{0\mathrm{T/q,Andreas}}$ (P5)	$C_{\mathrm{Ri_b}}$	◇	11.0	6.0	4
	$z_{0\mathrm{v}} = z_{0\mathrm{T/q}} = 0.61\,\mathrm{mm}$ (P4)	$C_{\mathrm{Ri_b}}$	▽	18.0	6.3	5
	$z_{0\mathrm{v}} = z_{0\mathrm{T/q}} = 0.61\,\mathrm{mm}$ (P4)	C_{log}	▼	18.5	3.0	6
	$z_{0\mathrm{v,ec}}$, $z_{0\mathrm{T/q}} = 0.1\,z_{0\mathrm{v,ec}}$ (P2)	$C_{\mathrm{Ri_b}}$	□	20.5	4.0	7
	$z_{0\mathrm{v}} = 0.01\,\mathrm{m}$, $z_{0\mathrm{T/q}} = 0.1\,z_{0\mathrm{v}}$ (P3)	C_{log}	▲	22.0	8.8	8
	$z_{0\mathrm{v}} = 0.01\,\mathrm{m}$, $z_{0\mathrm{T/q}} = 0.1\,z_{0\mathrm{v}}$ (P3)	$C_{\mathrm{Ri_b}}$	△	23.0	7.8	9
	$z_{0\mathrm{v,ec}}$, $z_{0\mathrm{T/q}} = 0.1\,z_{0\mathrm{v,ec}}$ (P2)	C_{log}	■	23.5	5.3	10

(Neustift, P2–C_{log}). For latent heat flux, RMSE varies between $1.9\,\mathrm{W\,m^{-2}}$ (Monte Bondone, P1–C_{log}) and $82.4\,\mathrm{W\,m^{-2}}$ (Alp Weissenstein, P3–C_{log}). A similarly wide spread is evident in the mean bias error. For Q_{H}, MBE ranges from $-137.5\,\mathrm{W\,m^{-2}}$ (Neustift, P1–C_{Rib}) to $51.6\,\mathrm{W\,m^{-2}}$ (Neustift, P2–C_{log}), while for Q_{L}, MBE spans from $-27.8\,\mathrm{W\,m^{-2}}$ (Neustift, P4–C_{Rib}) to $60.7\,\mathrm{W\,m^{-2}}$ (Mazia Pasture, P2–C_{log}). However, despite this wide spread, Fig. 9 does not show a clear trend with slope: RMSE, MBE, and Pearson r for both sensible and latent heat fluxes do not systematically increase or become more variable at steeper sites, indicating that model performance is largely independent of terrain inclination.

https://doi.org/10.5194/egusphere-2026-3417
Preprint. Discussion started: 29 July 2026

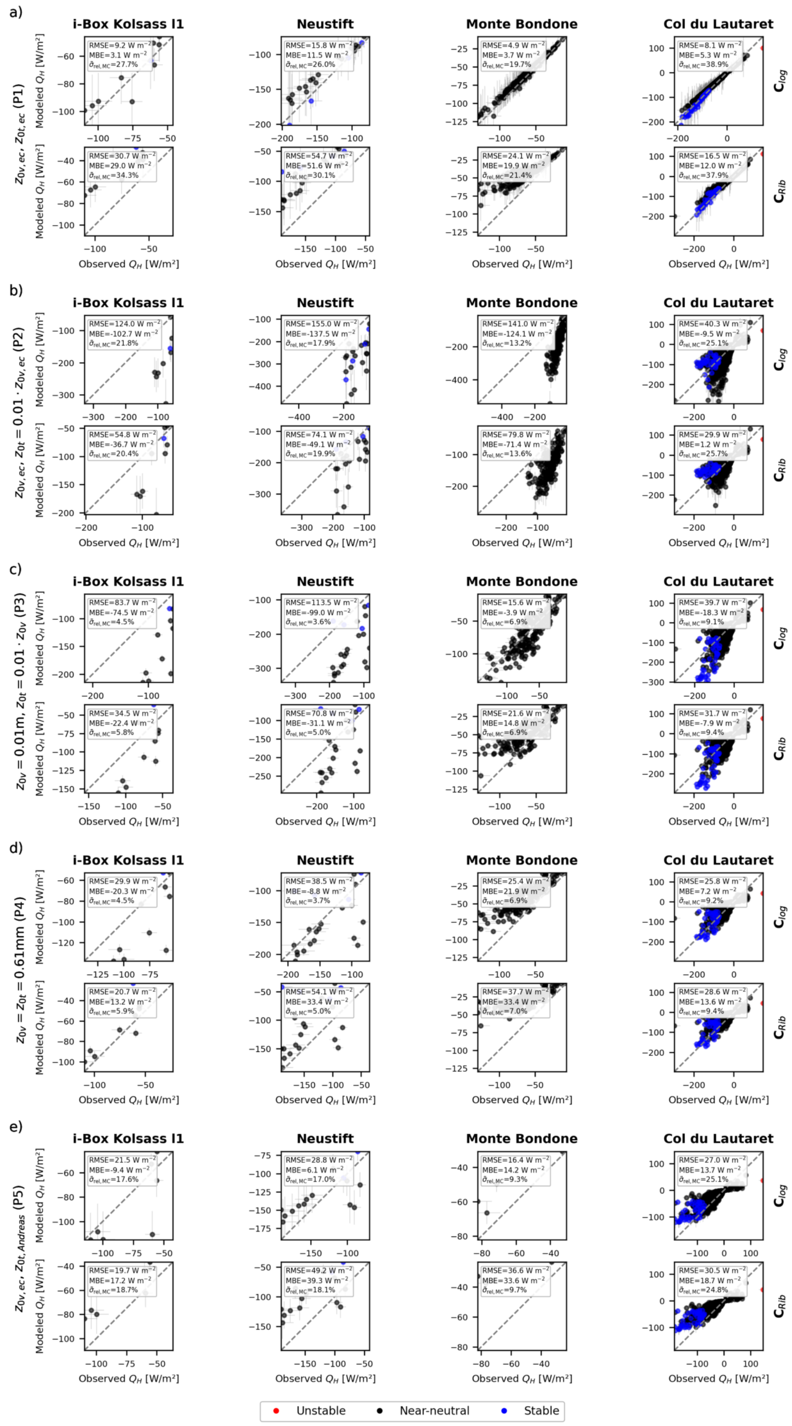

Figure 5. Scatterplots of modeled versus measured turbulent sensible heat fluxes for EC stations on slopes between $0.5°$ and $4.0°$, shown for all five z_0 parameterizations (blocks a–e) and both BA approaches (rows within each block). Colors indicate atmospheric stability: near-neutral ($|\zeta| \leq 0.1$, black), unstable (red), and stable (blue). Error bars indicate uncertainties in Q_{H} and Q_{L} resulting from error propagation described in Section 4.2.

https://doi.org/10.5194/egusphere-2026-3417
Preprint. Discussion started: 29 July 2026

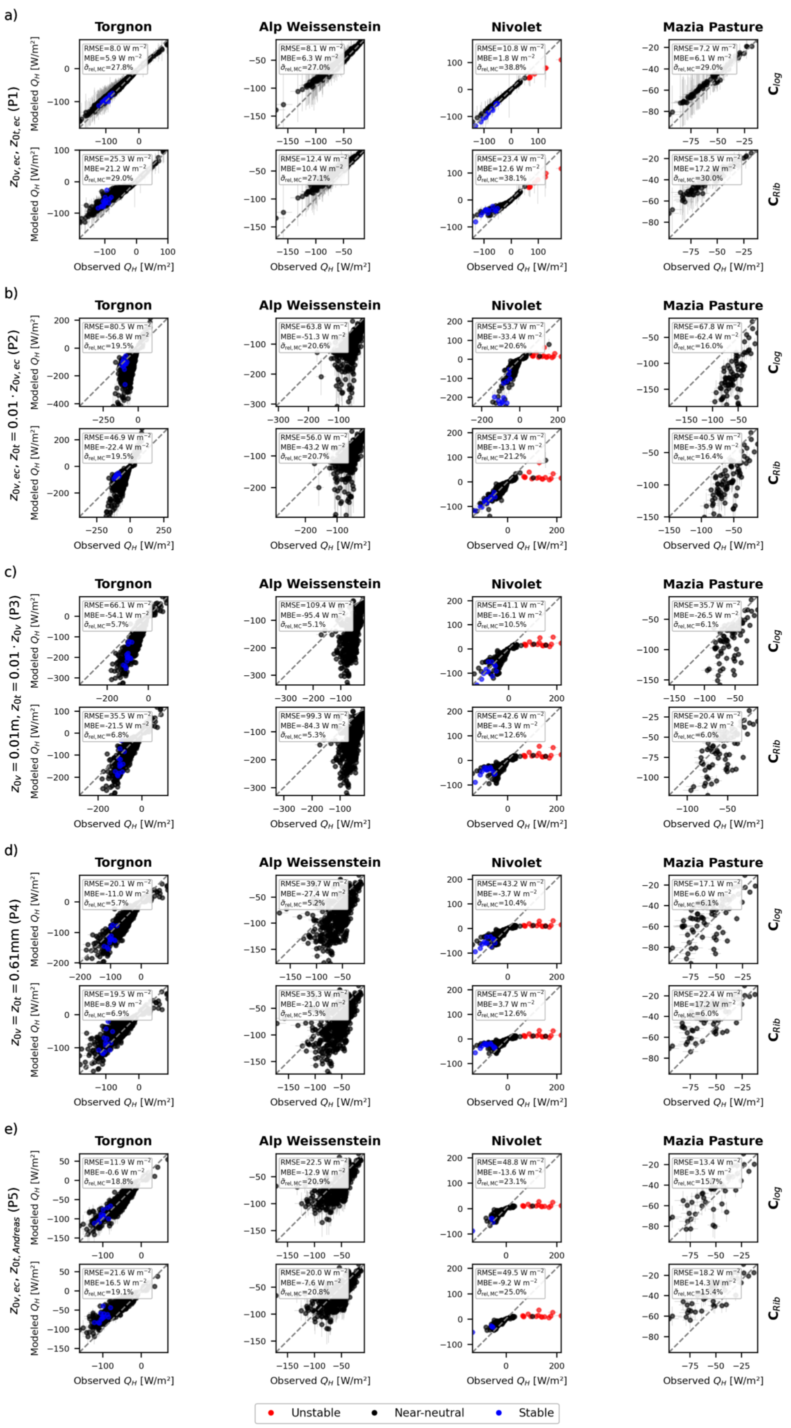

Figure 6. Same as Fig. 5, but for stations on slopes between 6.6° and 27.0°.

https://doi.org/10.5194/egusphere-2026-3417
Preprint. Discussion started: 29 July 2026

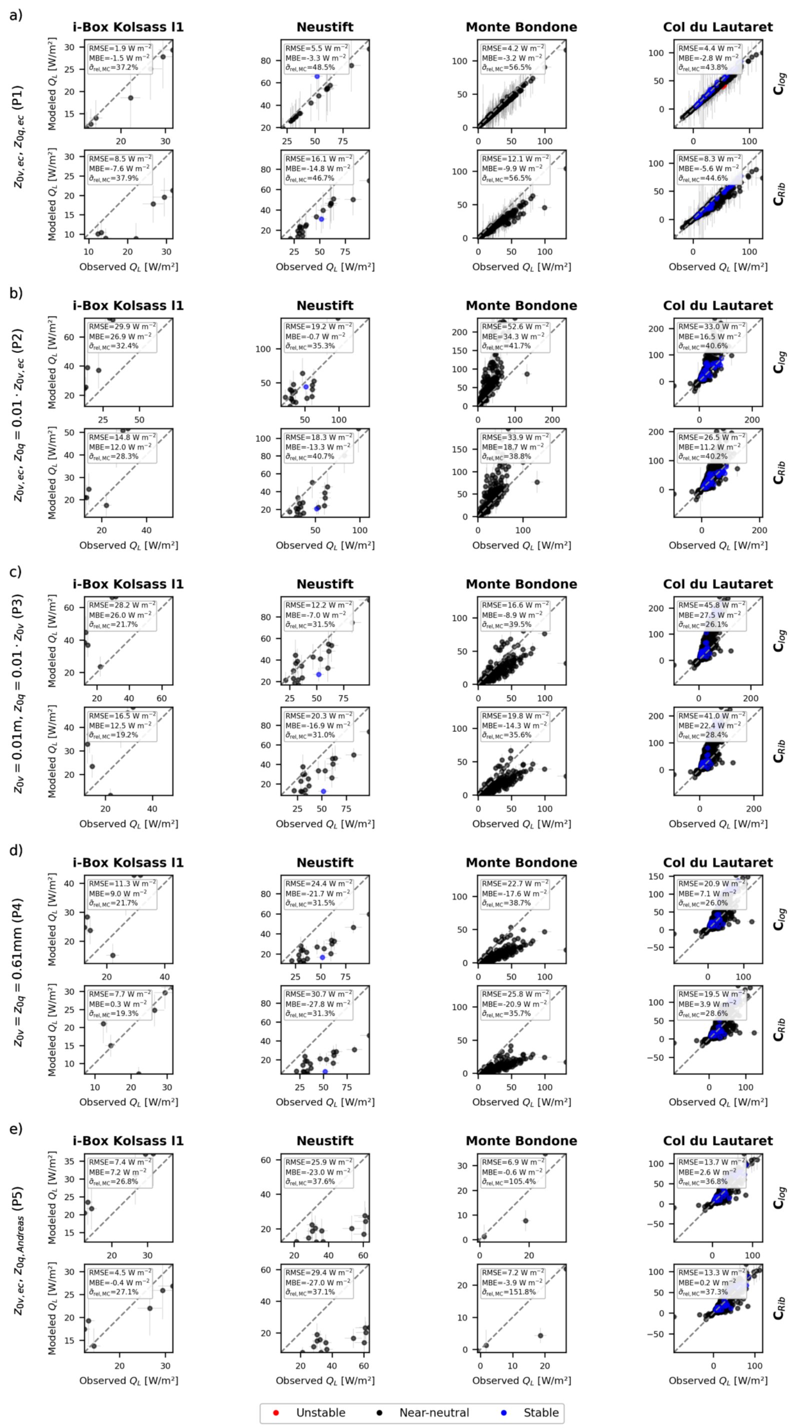

Figure 7. Same as Fig. 5, but for latent heat fluxes between 0.5° and 4.0°.

https://doi.org/10.5194/egusphere-2026-3417
Preprint. Discussion started: 29 July 2026

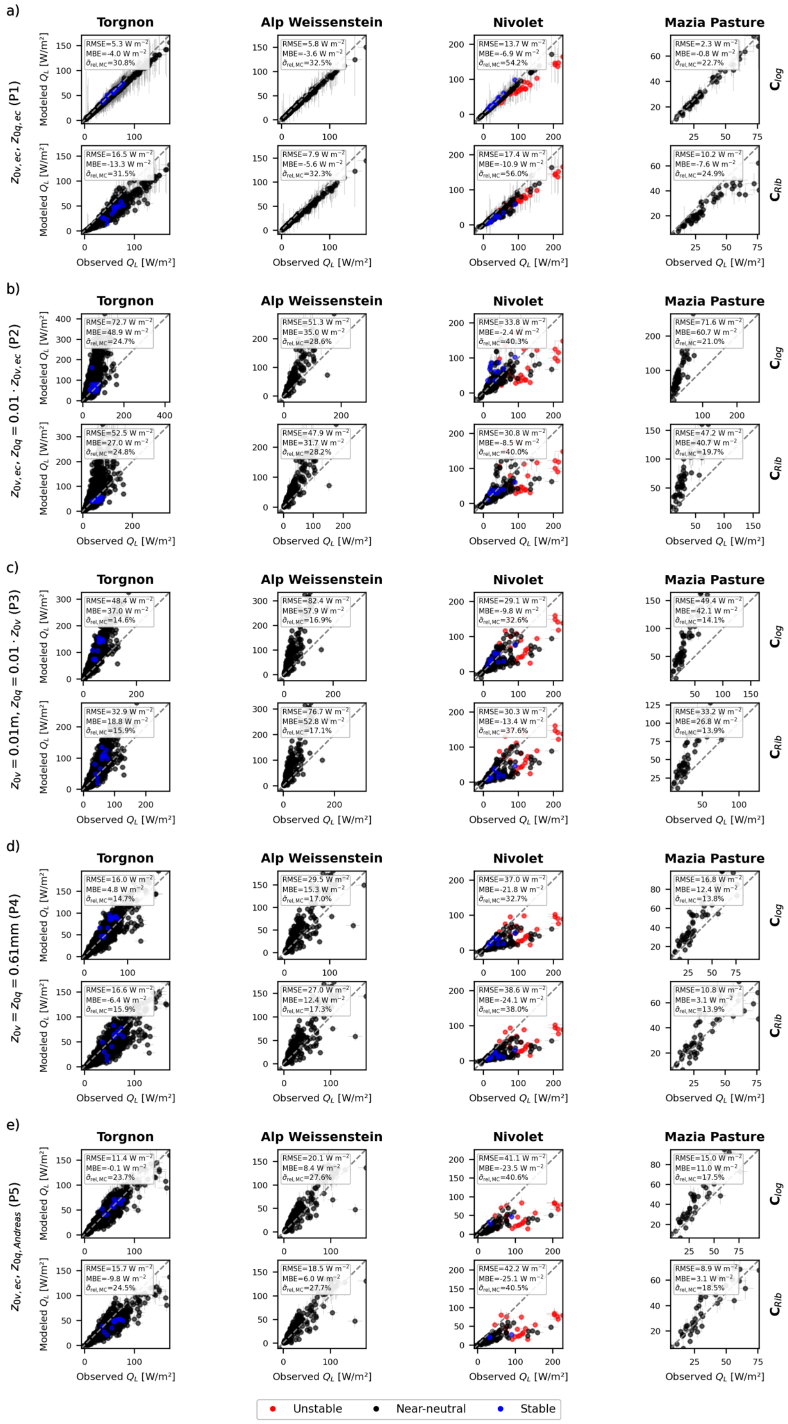

Figure 8. Same as Fig. 7, but for stations on larger slopes between 6.6° and 27.0°.

https://doi.org/10.5194/egusphere-2026-3417
Preprint. Discussion started: 29 July 2026

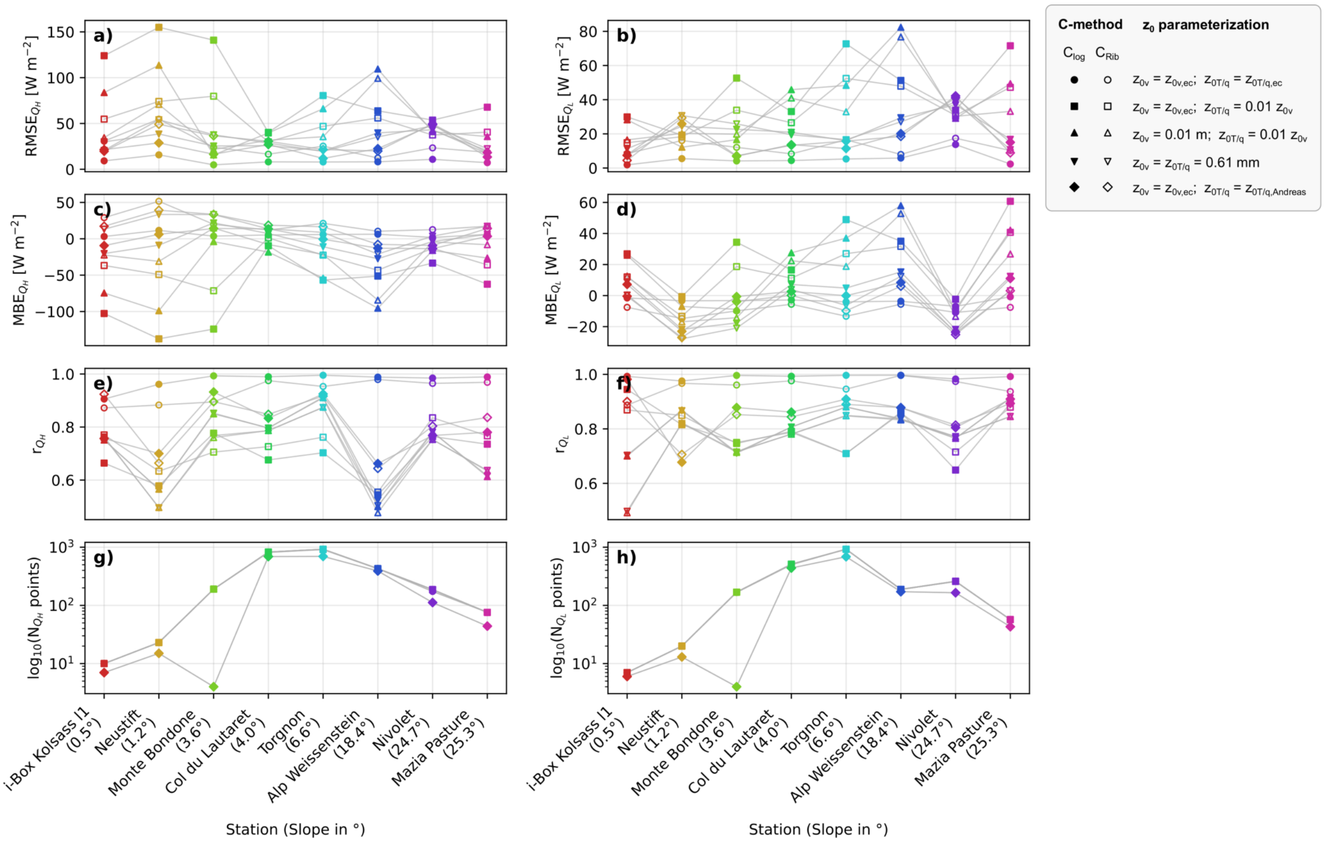

Figure 9. Summary of RMSE, MBE, Pearson correlation coefficient, and the number of available data points for turbulent sensible and latent heat fluxes at all stations. Stations are ordered by increasing slope angle. Panels (a)–(f) show RMSE, MBE, and the Pearson correlation coefficient for each station (color-coded) for all combinations of z_0 parameterizations (different symbols) and BA methods (filled symbols for $C_{\log}$, open symbols for C_{Rib}). Panels (a,c,e) correspond to turbulent sensible heat fluxes, panels (b,d,f) to turbulent latent heat fluxes. Panels (g) and (h) indicate the number of data points available for the analysis at each station for sensible and latent heat fluxes for each possible combination.

https://doi.org/10.5194/egusphere-2026-3417
Preprint. Discussion started: 29 July 2026

5 Discussion

In this section, we interpret our findings regarding the applicability of the law of the wall in complex terrain (Section 5.1) and the sensitivity of derived roughness lengths and turbulent heat fluxes to measurement uncertainties (Section 5.1.1). In Section 5.1.2, we further discuss the performance of different combinations of BA methods and z_0 parameterizations across sites with varying slope characteristics.

5.1 Law of the wall

The applicability of the classical law of the wall is a key assumption underlying roughness length estimation in bulk flux modeling. In complex mountainous terrain, deviations from logarithmic wind profiles can arise from terrain-induced flow distortion, slope, and local surface heterogeneity. At the flat i-Box Kolsass site, roughness lengths derived from different measurement heights are generally consistent, particularly during December 2017, although some temporal variability remains. In February 2020, larger differences are observed across all levels, indicating that even in a relatively wide, flat valley, the assumptions underlying logarithmic wind profiles can be violated.

At the sloping i-Box Hochhäuser site, discrepancies between measurement levels are substantially larger and persist across all investigated periods and methods. This behavior indicates a systematic violation of the assumptions underlying the law of the wall. To assess whether these discrepancies could be related to differences in the surface areas contributing to the measured fluxes, flux footprint climatologies were calculated for the investigated time periods.

At the flat i-Box Kolsass site, the strong overlap of footprints across measurement heights and the homogeneous land cover suggest that inter-level differences in $z_{0\mathrm{v}}$ cannot be attributed to variations in source area or surface type. This supports the interpretation that deviations from the logarithmic wind profile at this site are primarily related to measurement height and temporal variability rather than footprint heterogeneity.

At the sloping i-Box Hochhäuser site, footprints vary more strongly with measurement height. In particular, the footprint of the upper measurement level partially extends towards forested terrain within the outer footprint contours (approximately the $80\,\%$ to $90\,\%$ cumulative contribution). This indicates that the higher measurement level samples a slightly more heterogeneous surface, which could potentially contribute to larger roughness length estimates. To assess this effect, wind directions associated with increased forest contributions within the footprint were analyzed separately (Appendix B). However, these cases do not yield systematically higher $z_{0\mathrm{v}}$ values. This suggests that the limited forest contribution evident in Fig. 3 does not provide a consistent explanation for the observed inter-level differences.

The pronounced discrepancies between measurement levels and the strong temporal variability in $z_{0\mathrm{v}}$ at i-Box Hochhäuser instead point towards terrain-induced flow distortion. Although periods with the upper measurement level above the low-level jet maximum were excluded, the flow at this site is likely still influenced by larger-scale valley wind systems. In addition, different flow processes may affect the measurement levels unequally–for example, slope winds may dominate at the lowest level, while a combination of slope and valley winds influences the upper level. Such vertically heterogeneous flow regimes violate the assumptions underlying the logarithmic wind profile. Under these conditions, the assumption of a horizontally

https://doi.org/10.5194/egusphere-2026-3417
Preprint. Discussion started: 29 July 2026

homogeneous surface layer is not fulfilled, rendering roughness lengths derived from single-level EC measurements highly sensitive to sensor height.

Overall, our findings imply that momentum roughness lengths for snow derived from EC observations in mountainous terrain should be interpreted with caution, particularly on slopes. While the law of the wall yields partially reasonable estimates at the flat i-Box Kolsass site under near-neutral conditions, this behavior is limited to specific periods only. Even in the context of a wide, flat mountain valley, where i-Box Kolsass is located, substantial deviations from logarithmic wind profiles occur during some periods, indicating that the direct application of the law of the wall is of limited reliability not only on slopes but also in flat terrain embedded within complex topography.

An important indication of the limitations of momentum roughness length estimates under these conditions is the inconsistency between different derivation methods. Under identical, fully or partially snow-covered conditions, the applied approaches yielded values ranging from sub-millimeter to centimeter scales. In principle, if the wind profile followed a logarithmic form, roughness lengths derived from different measurement levels and from profile-based fits should converge to similar values. The observed discrepancies therefore indicate a violation of the logarithmic wind profile assumption, likely due to terrain-induced flow distortion and vertically heterogeneous flow regimes. The even larger spread obtained from regression-based approaches may further reflect the combination of data from differing flow conditions. Consequently, the large variability in $z_{0\mathrm{v}}$ does not represent independent uncertainty, but rather highlights that the concept of a single, well-defined roughness length is not robust under these complex conditions.

5.1.1 Error propagation

In the first step of the sensitivity analysis, we examined how measurement and instrumental uncertainties propagate into roughness lengths calculated under near-neutral conditions. Overall, relative uncertainties are substantial for both momentum and scalar roughness lengths (Table 5). However, uncertainties in momentum roughness length are generally smaller and typically remain below $70\,\%$, whereas scalar roughness lengths, particularly $z_{0\mathrm{T}}$, exhibit much larger uncertainties and often exceed $100\,\%$. Figures A2 and A3 further show that even small errors in scalar differences can produce large variations in the estimated scalar roughness lengths. This highlights the high sensitivity of scalar roughness length retrieval to measurement uncertainty.

The Monte Carlo analysis shows that the typical propagated uncertainty in modeled turbulent fluxes is substantial, particularly for latent heat flux and for parameterizations that directly use EC- derived scalar roughness lengths. Using the relative uncertainty metric $\tilde{\sigma}_{\mathrm{rel,MC}}$, the largest values are obtained for P1, with propagated uncertainties of about $19.7\,\%$ to $38.9\,\%$ for Q_{H} and $22.7\,\%$ to $56.5\,\%$ for Q_{L}. This indicates that flux estimates based directly on EC-derived $z_{0\mathrm{T}}$ and $z_{0\mathrm{q}}$ remain highly sensitive to uncertainty in the underlying roughness length estimates. More generally, the larger propagated uncertainties found for Q_{L} suggest that latent heat flux estimates are more sensitive than sensible heat flux estimates to uncertainty in the scalar exchange formulation. This is consistent with the large variability and limited observational support of $z_{0\mathrm{q}}$ found in the first step of the sensitivity analysis.

Beyond the propagated flux uncertainties, the absolute magnitude and variability of the retrieved roughness lengths also merit discussion. The momentum roughness lengths calculated for near-neutral conditions range from $1.66\,\mathrm{cm}$ to $54.95\,\mathrm{cm}$,

https://doi.org/10.5194/egusphere-2026-3417
Preprint. Discussion started: 29 July 2026

placing them at the upper end of $z_{0\mathrm{v}}$ values reported for snow (Brock et al., 2006). Such large values may partly reflect local site characteristics within the upwind fetch, including nearby forests, grassland, pasture, and complex terrain, rather than the snow surface alone. The footprint climatologies (Fig. C1) support this interpretation for some stations, such as i-Box Eggen, i-Box Hochhäuser, and Nivolet. However, fetch characteristics alone do not fully explain the observed variability, as relatively high mean $z_{0\mathrm{v}}$ values also occur at sites located on comparatively flat terrain, such as i-Box Kolsass and Neustift. As discussed in Section 5.1, another likely explanation is that violations of the law of the wall in complex terrain contribute to elevated and height-dependent momentum roughness lengths. In addition, the relative uncertainties in $z_{0\mathrm{v}}$ itself reach up to $70\,\%$, which likely explains part of the observed inter-site variability.

Even though the mean values of $z_{0\mathrm{v}}$ are of similar order of magnitude to those commonly prescribed in snow models such as FSM2 (Essery, 2015) and openAmundsen (Strasser et al., 2024), which typically assume a momentum roughness length of $1\,\mathrm{cm}$ for snow surfaces, our results do not support the widespread assumption of a fixed ratio $z_{0\mathrm{T/q}} = 0.1\,z_{0\mathrm{v}}$. The mean scalar roughness lengths derived for individual stations differ strongly from this relationship and also show no consistent relationship to one another (Table 5). This suggests that fixed scalar-to-momentum roughness ratios may substantially underestimate the uncertainty associated with turbulent heat flux estimates over seasonal snow.

5.1.2 Comparison of BA formulations and z_0 parameterizations

Overall, the best agreement between modeled and measured turbulent fluxes is obtained using the $C_{\log}$ formulation in combination with EC-derived roughness lengths for momentum, temperature, and humidity. This result is expected, as the $C_{\log}$ approach essentially represents an inversion of the procedure used to derive these roughness lengths from the observed fluxes. The remaining deviations, particularly under unstable conditions such as those at the Nivolet station, can be attributed to the absence of explicit stability corrections in the $C_{\log}$ formulation. In contrast, larger discrepancies are anticipated when combining the first z_0 parameterization with the C_{Rib} formulation, since its stability correction depends on the bulk Richardson number (Eq. 22) rather than on ζ. Consequently, stability corrections are also applied in cases previously classified as near-neutral ($|\zeta| \leq 0.1$), which explains the increased deviations observed for these conditions.

The ranking of the performance of the different BA and z_0 formulations indicates that the poorest performance is obtained for both BA formulations when combined with a z_0 parameterization that assumes a constant ratio between $z_{0\mathrm{v}}$ and $z_{0\mathrm{T/q}}$ ($z_{0\mathrm{T/q}} = 0.1\,z_{0\mathrm{v}}$). As shown in Table 5, this ratio is rarely supported by the observations, with $z_{0\mathrm{v}}$ and $z_{0\mathrm{q/T}}$ differing by one to three orders of magnitude. Consistent with this finding, the performance metrics presented in Figures 5–9 further demonstrate that assuming a fixed ratio of 1/10 leads to systematically degraded model performance. We therefore conclude that this commonly used ratio in snow models is not an adequate choice for representing scalar roughness lengths at the studied sites presented in this work.

Apart from using EC-derived roughness lengths directly, the best performance is achieved with the surface renewal model of Andreas (1987), which was developed specifically for ice, snow, and ocean surfaces and explicitly accounts for intermittent near-surface turbulence. However, the applicability of the surface renewal model is limited in practice, as the number of available data points is reduced, in some cases substantially (e.g. at the Monte Bondone site) when calculating scalar roughness

https://doi.org/10.5194/egusphere-2026-3417
Preprint. Discussion started: 29 July 2026

lengths. Moreover, its continued dependence on the EC-derived momentum roughness length, $z_{0\mathrm{v,ec}}$, further constrains its suitability for applications such as snow models, where such information is typically unavailable.

Among the z_0 parameterizations that are independent of EC-derived estimates, the best performance is obtained by assuming a constant roughness length equal for momentum, temperature, and humidity. Given that $z_{0\mathrm{v}}$, $z_{0\mathrm{T}}$, and $z_{0\mathrm{q}}$ were shown to differ substantially from each other, this result is noteworthy and likely reflects a compensation of errors, whereby over- and underestimation of the individual roughness lengths partly cancel out within the bulk flux formulation. Nevertheless, the remaining errors are still substantial, indicating that this approach should be regarded as a pragmatic rather than physically realistic representation of turbulent exchange over snow and ice surfaces.

A comparison of the two BA formulations further reveals that neither clearly outperforms the other. Although the C_{Rib} formulation includes stability correction functions, these do not result in a systematic improvement of the modeled turbulent fluxes. This finding is consistent with earlier studies e.g., Braithwaite (1995); Hock (2005); Herrero et al. (2009) reporting that the introduction of stability correction functions does not necessarily lead to improved flux estimates.

Overall, the results suggest that the choice of z_0 parameterization has a stronger influence on model performance than the choice of BA formulation among the two approaches considered. This is evident from Fig. 10, where results obtained with the same z_0 parameterization (indicated by identical symbol shapes) tend to cluster closely together, regardless of whether filled or unfilled symbols are used to distinguish between the two BA formulations. In contrast, a substantially larger spread is observed between different symbol shapes, reflecting the variability introduced by the choice of z_0. This pattern indicates that model sensitivity to roughness parameterization exceeds that associated with the choice of BA method.

Despite the presence of substantial slopes at the study sites, reaching up to 25.3° at Mazia Pasture station, model performance does not show a systematic dependence on slope. This finding is consistent with the results of Sfyri et al. (2018), who likewise did not observe a systematic dependence of scaling relations on slope. This suggests that, for the BA formulations and z_0 parameterizations considered here, topographic effects are secondary compared with the influence of surface roughness representation. The dominance of roughness length errors likely masks potential slope-related impacts on turbulent fluxes, implying that further improvements in z_0 parameterizations may be more effective for enhancing model accuracy than explicit slope corrections in these contexts.

5.2 Limitations of the study

A primary limitation of this study is the reduction in available data after applying the relatively strict quality filters. Although several years of measurements were available across multiple sites, only a small subset of data points met all criteria for inclusion in the analysis. This reduces the statistical robustness at some sites and, in certain cases, even led to an incomplete analysis–for example, at i-Box Eggen, i-Box Hochhäuser, i-Box Weerberg, and Früebüel.

One filter that particularly contributed to the reduction in available data points is the surface temperature filter. As discussed in Section 3.3, surface temperatures derived from net longwave radiation are especially prone to errors, which can strongly affect the calculation of scalar roughness lengths for temperature and humidity. For this study, we selected periods where the surface temperature $T_{\mathrm{S}} = 0\,^\circ\mathrm{C}$. This constraint substantially reduced the number of usable data points and restricted the

https://doi.org/10.5194/egusphere-2026-3417
Preprint. Discussion started: 29 July 2026

analysis primarily to the melting period of the snowpack. Consequently, the study is limited in its ability to examine snow in other phases of metamorphism and to investigate the temporal evolution of snow roughness lengths.

This study focuses on comparing parameterizations for turbulent heat fluxes commonly used in snow models, but does not include a direct comparison between measured fluxes and fluxes simulated by the snow models themselves. This was a deliberate choice to isolate the sensitivity of flux calculations to uncertainties in the available meteorological input data, without introducing additional uncertainty from the physical modeling of other snow processes. A potential direction for future research would be to investigate how the uncertainties identified in this study propagate into modeled turbulent fluxes within snow models and, in turn, how they affect key snowpack properties, such as snow water equivalent.

6 Conclusions

In this study, we evaluated how measurement uncertainty, roughness length parameterization, and the validity of MOST affect aerodynamic roughness lengths and modeled turbulent heat fluxes over seasonal snow in complex terrain. Using data from twelve EC stations across the Alps, including two multi-level towers, we combined analyses of law-of-the-wall validity, roughness length uncertainty, and BA-model performance across a range of slopes and site conditions.

The results show that roughness lengths derived from EC observations are highly sensitive to both measurement uncertainty and theoretical assumptions. At the multi-level towers, momentum roughness lengths derived under near-neutral conditions varied by up to one order of magnitude between measurement heights, indicating that the retrieval of a unique $z_{0\mathrm{v}}$ is not robust even under conditions where logarithmic wind profiles would be expected. This suggests that, in complex terrain, uncertainty in roughness length does not arise only from measurement noise, but also from violations of the assumptions underlying the law of the wall and MOST.

The sensitivity analysis demonstrated that instrumental and measurement uncertainties can strongly influence calculated roughness lengths from turbulent fluxes, especially scalar roughness lengths, which exhibited large relative errors. These effects are particularly pronounced under the predominantly observed near-neutral or stable conditions, where small vertical gradients in temperature and humidity amplify the impact of measurement uncertainty. As a result, these uncertainties propagate into modeled turbulent fluxes, producing relative errors of up to $56.5\,\%$ for Q_{L} and up to $38.9\,\%$ for Q_{H}, with large contributions stemming from uncertainties in roughness length.

We also found substantial variation among sites in the roughness lengths for momentum, temperature, and humidity, as well as in the ratios between momentum and scalar roughness lengths. Notably, the commonly assumed fixed ratio (1/10) between z_{0v} and $z_{0T/q}$ did not hold, which explains the poor performance of parameterizations that rely on this assumption.

Among the tested BA methods and z_0 parameterizations, no approach exhibited systematically worse performance with increasing slope. This suggests that, although MOST has known limitations in complex terrain, slope itself does not control the performance of BA methods. Rather, the challenges appear to arise from the general application of MOST in complex terrain. Furthermore, consistent with findings from previous studies, we observed that stability corrections do not consistently improve modeled fluxes.

https://doi.org/10.5194/egusphere-2026-3417
Preprint. Discussion started: 29 July 2026

Overall, the main contribution of this study is to show that uncertainty in BA-based turbulent flux estimates over seasonal snow in complex terrain arises not only from imperfect measurements, but also from the limited robustness of the roughness length concept itself when MOST assumptions are weakly satisfied.

Code availability. The scripts used for data processing and analysis are available from the corresponding author upon request.

https://doi.org/10.5194/egusphere-2026-3417
Preprint. Discussion started: 29 July 2026

Appendix A: Sensitivity analysis on roughness lengths

The relative uncertainties of $z_{0\mathrm{v}}$, $z_{0\mathrm{T}}$ and $z_{0\mathrm{q}}$ in dependency of u, u_*, ΔT, θ_*, Δq and q_* are visualized in Figs. A1-A3. The calculated relative errors here are only calculated from uncertainties in u, u_*, ΔT, θ_*, Δq and q_*, for visualization purposes. Uncertainties in z_u and $z_{\mathrm{T/q}}$ are excluded.

https://doi.org/10.5194/egusphere-2026-3417
Preprint. Discussion started: 29 July 2026

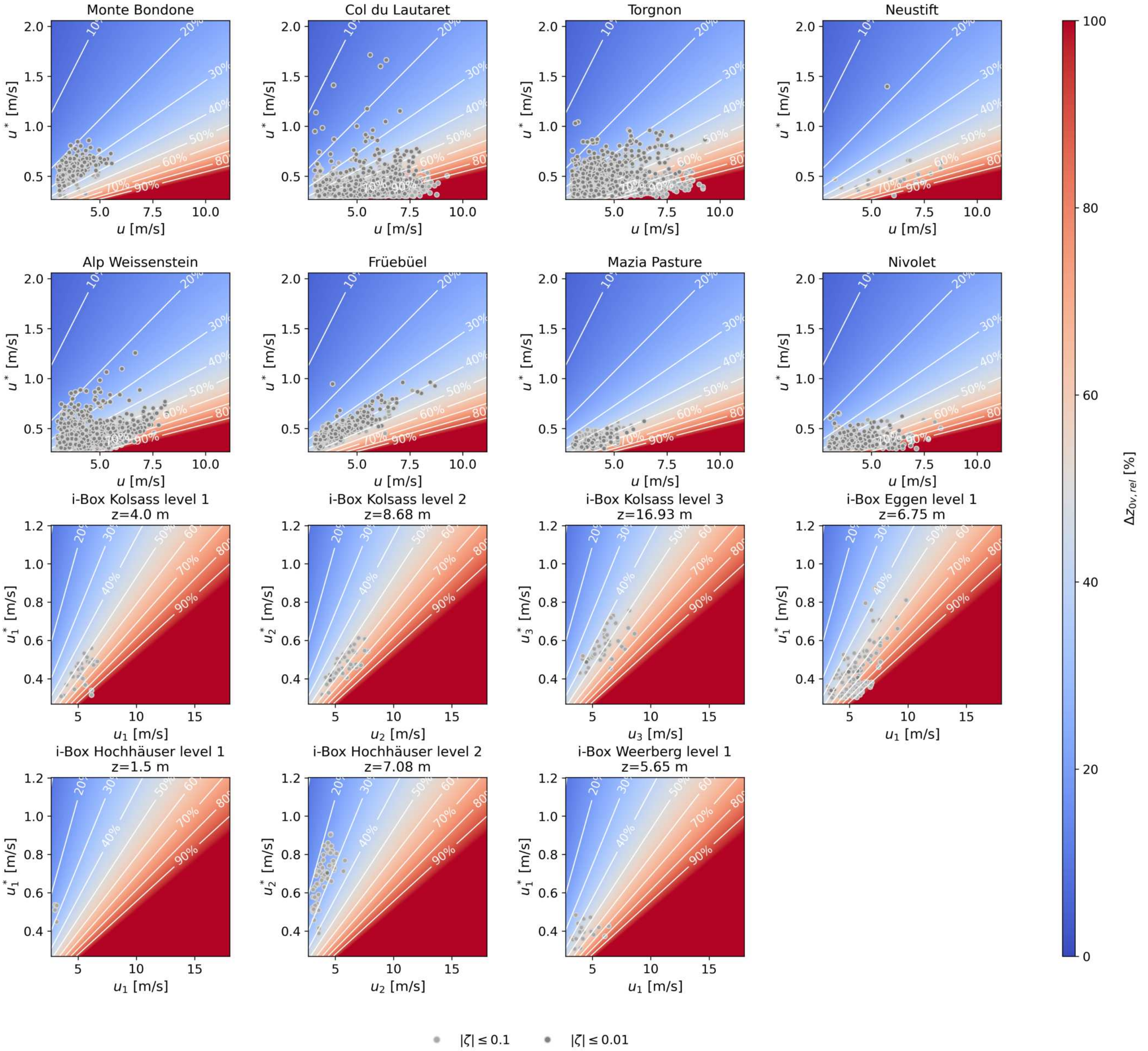

Figure A1. Relative uncertainty of the momentum roughness length $z_{0\mathrm{v}}$ for all stations and data points, shown for two stability regimes ($|\zeta| \leq 0.01$ and $|\zeta| \leq 0.1$). Only wind speed and friction velocity uncertainties are included; instrument height uncertainties are neglected in the calculation of total uncertainties in this Figure.

https://doi.org/10.5194/egusphere-2026-3417
Preprint. Discussion started: 29 July 2026

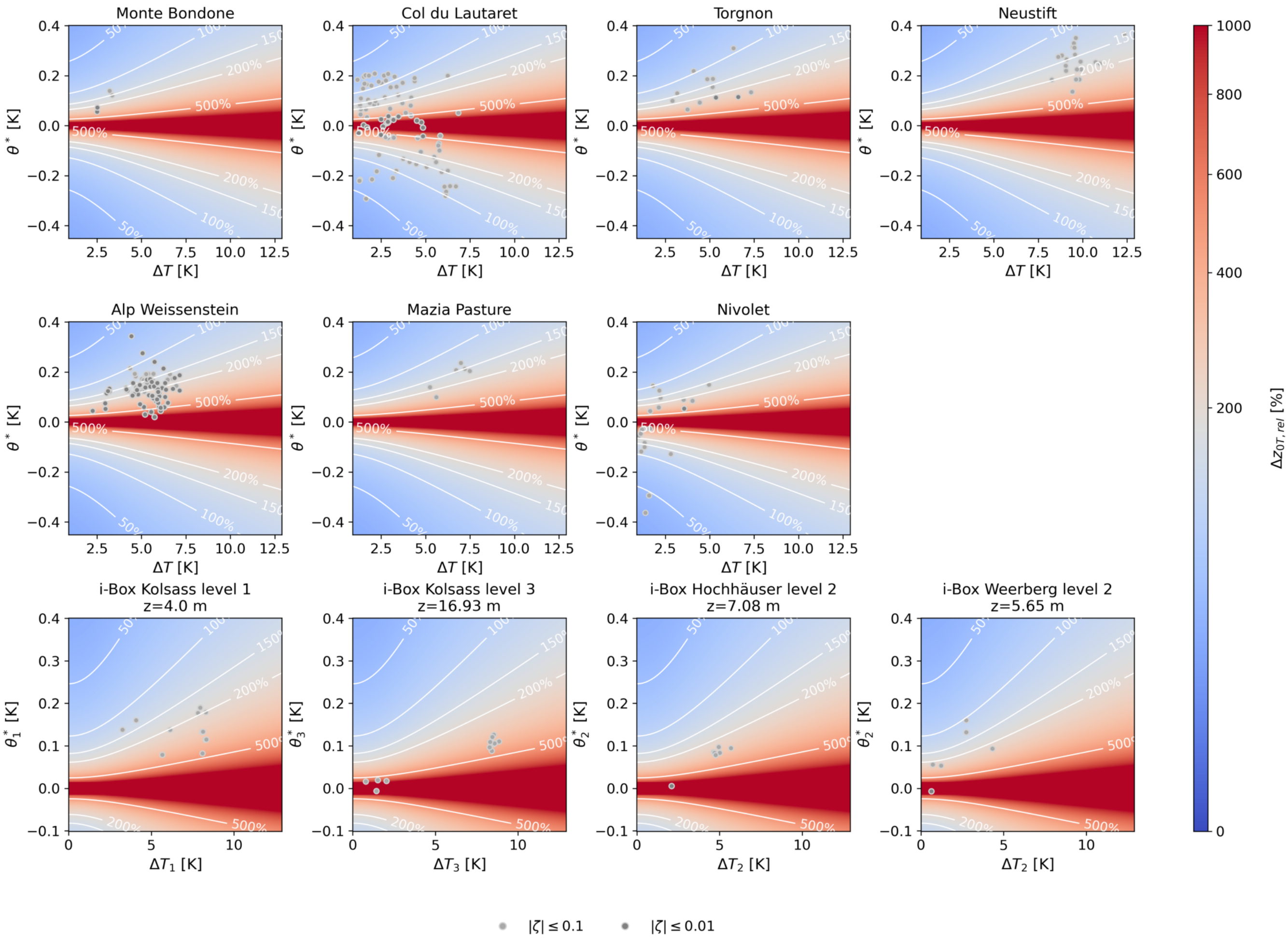

Figure A2. Relative uncertainty of the thermal roughness length $z_{0\mathrm{T}}$ for all stations and data points, shown for two stability regimes. Only uncertainties in temperature difference ΔT and temperature scale θ_* are included; instrument height uncertainties are neglected in the calculation of total uncertainties in this Figure.

https://doi.org/10.5194/egusphere-2026-3417
Preprint. Discussion started: 29 July 2026

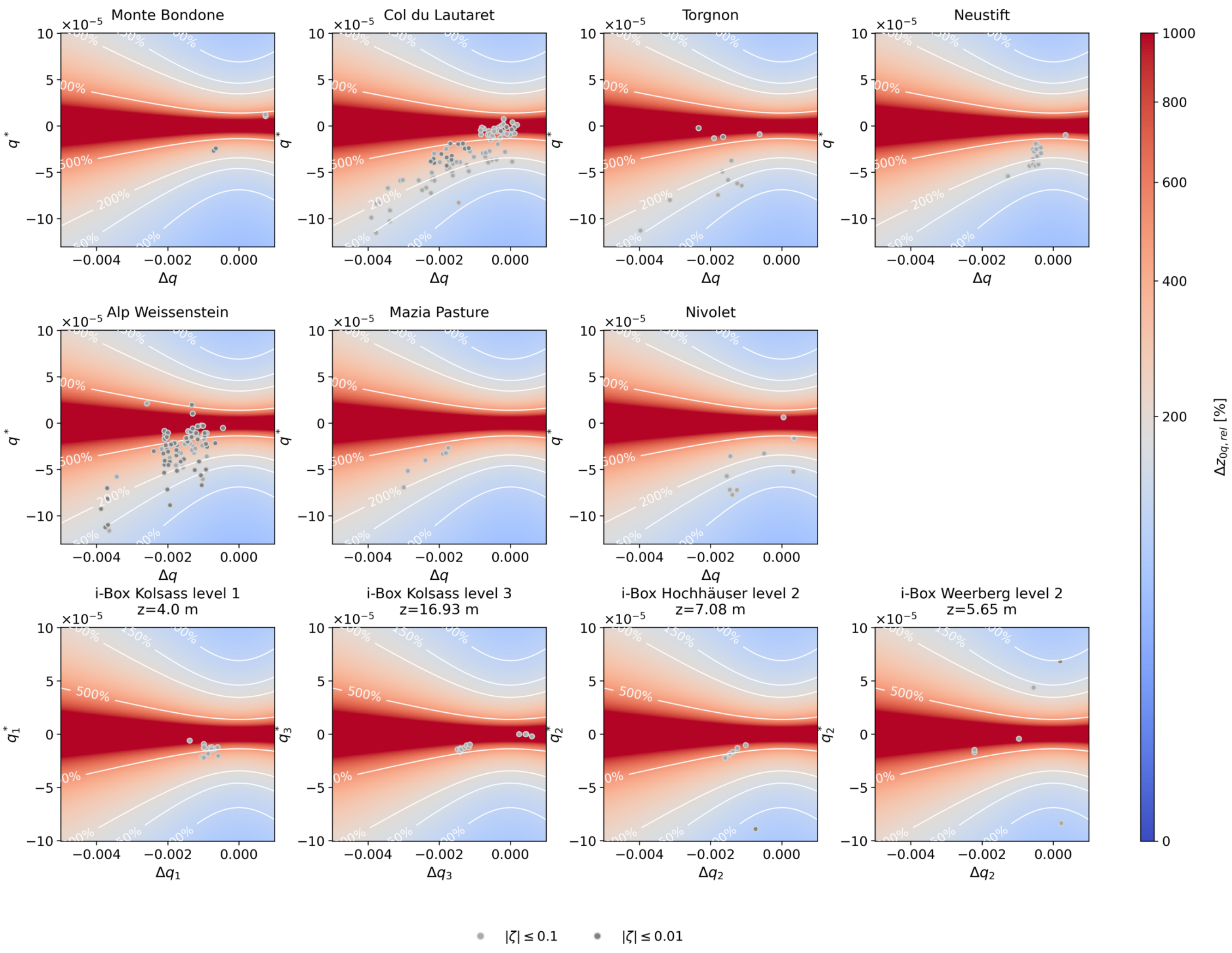

Figure A3. Relative uncertainty of the moisture roughness length z_{0q} for all stations and data points, shown for two stability regimes. Only uncertainties in humidity difference Δq and humidity scale q_* are included; instrument height uncertainties are neglected in the calculation of total uncertainties in this Figure.

https://doi.org/10.5194/egusphere-2026-3417
Preprint. Discussion started: 29 July 2026

Appendix B: Footprint climatology at i-Box Hochhäuser

To assess whether the elevated roughness lengths derived for the second measurement level at i-Box Hochhäuser can be attributed to increased land-cover heterogeneity within the corresponding flux footprint, footprint climatologies were calculated for two dominant wind-direction sectors. These sectors were selected to represent differing degrees of forest influence within the footprint.

Flux footprint climatologies for two main wind directions (250° and 180°) are displayed in Fig. B1.

Even though the footprint for 250° covers more area over forest, calculated roughness lengths are not higher with respect to the roughness lengths calculated with the footprint with wind directions centered around 180° covering less forest.

Fig. B1 shows flux footprint climatologies for wind directions centered around 180° (a) and 250° (b), respectively. For wind directions around 180°, the region contributing the dominant fraction of the measured flux is largely confined to grassland, while forested areas are mainly included within the outer footprint contours corresponding to higher cumulative contributions (approximately 80 % to 90 %). In contrast, for wind directions around 250°, forested terrain is already encompassed within footprint regions associated with lower cumulative contributions (approximately 50 % to 80 %), indicating a stronger forest influence within the effective source area.

Despite the increased forest contribution in the latter case, the roughness lengths derived for wind directions centered around 250° are not systematically larger than those obtained for wind directions centered around 180° (Fig. B2). This indicates that the higher roughness lengths observed at the upper measurement level cannot be explained solely by differences in land cover within the flux footprint.

This supports the interpretation presented in Sec. 5.1 that deviations from the law of the wall at i-Box Hochhäuser are primarily related to terrain-induced flow effects rather than footprint heterogeneity.

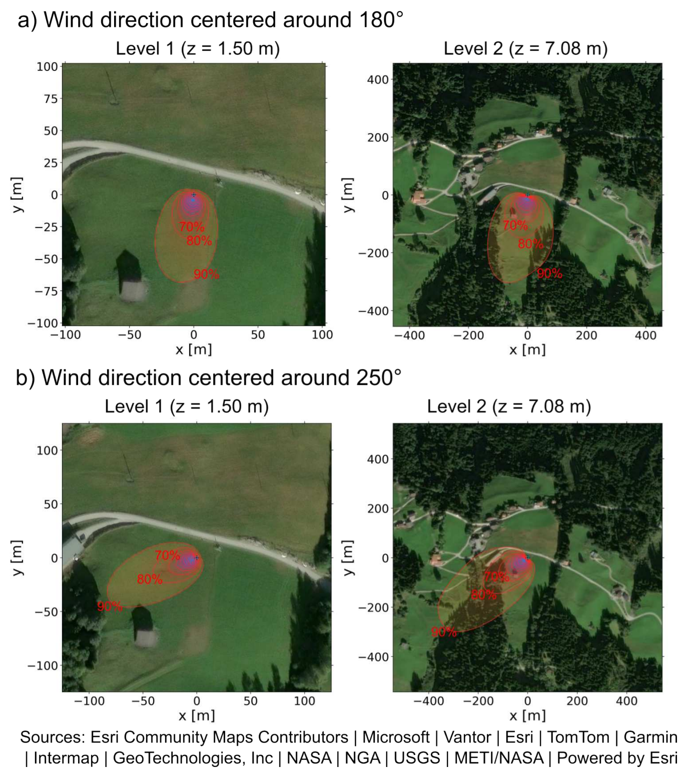

Figure B1. Flux footprints calculated for i-Box Hochhäuser for the two measurement levels filtered for different wind direction windows (a) main wind direction 180° (same as Fig. 3b), b) main wind direction 250°). Orthophoto basemap from Esri World Imagery (Esri, 2026).

https://doi.org/10.5194/egusphere-2026-3417
Preprint. Discussion started: 29 July 2026

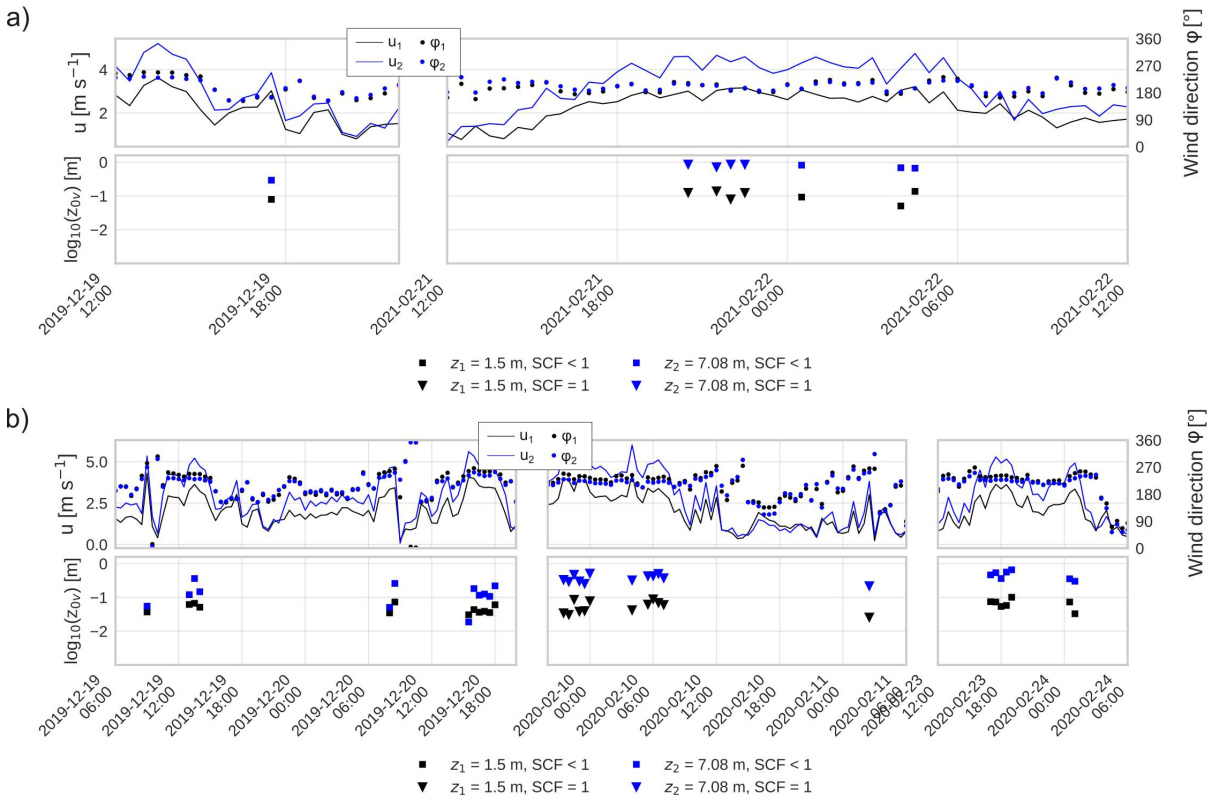

Figure B2. Comparison of roughness lengths calculated at i-Box Hochhäuser for (a) main wind direction 180° (same as Fig. 2b), b) main wind direction 250°).

https://doi.org/10.5194/egusphere-2026-3417
Preprint. Discussion started: 29 July 2026

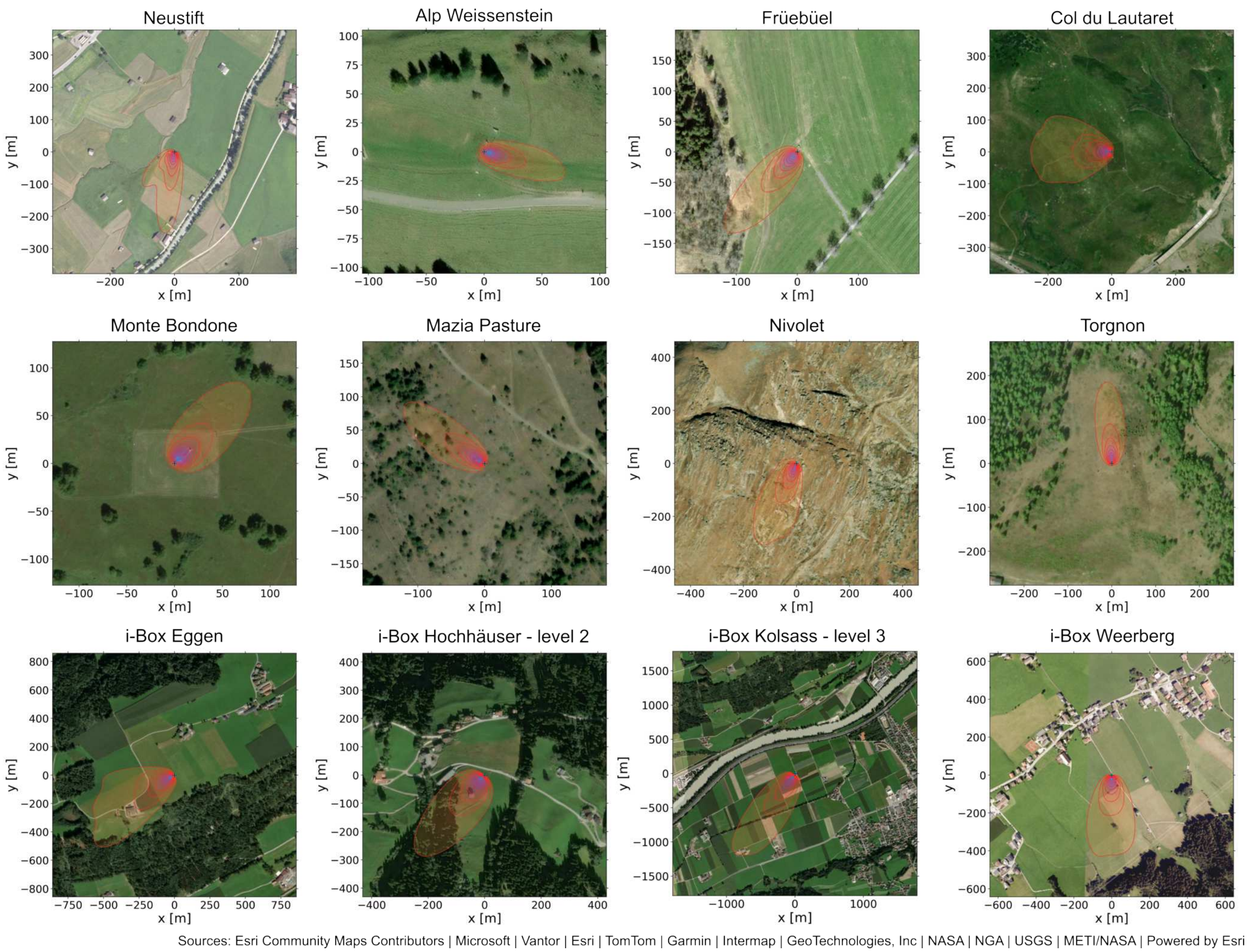

Figure C1. Footprints of EC stations averaged over the evaluated time steps fulfilling all quality criteria. Orthophoto basemap from Esri World Imagery (Esri, 2026).

Appendix C: EC station footprint climatology

EC footprints were calculated following Kljun et al. (2015). We averaged the footprints for each station over all data available after filtering. Since not all stations provide the full information needed to calculate the footprints according to Kljun et al. (2015), we needed to estimate some input parameters, which included most frequently σ_{v}, the standard deviation of the lateral wind speed. Here, we followed the parameterization suggested in Volk et al. (2023) who estimate $\sigma_{\mathrm{v}} = 1.9 \cdot u_{*}$. Figure C1 shows the average footprints for all stations, for EC stations with several measurement levels, like i-Box Kolsass and i-Box Hochhäuser, we showed the largest footprint corresponding to the footprint of the highest measurement level.

https://doi.org/10.5194/egusphere-2026-3417
Preprint. Discussion started: 29 July 2026

Author contributions. **Scheidt, K.T.:** Writing - original draft, Writing - review & editing, Conceptualization, Methodology, Data curation, Investigation, Validation, Software, Formal analysis, Visualization. **Pimentel, R.:** Writing - review & editing, Conceptualization, Supervision. **Deidda, P.:** Writing - review & editing, Data curation, Conceptualization. **Marin, C.:** Writing - review & editing, Conceptualization. **Gisolo, D.:** Writing - review & editing, Data curation. **Canone, D.:** Writing - review & editing, Data curation. **Polo, M.J.:** Supervision. **Notarnicola, C.:** Writing - review & editing, Supervision. **Lehner, M.:** Writing - review & editing, Data curation, Conceptualization, Methodology, Supervision.

Competing interests. The authors declare that they have no known competing financial interests or personal relationships that could have appeared to influence the work reported in this paper.

Acknowledgements. This work is part of the project PCI2024-153496, funded by MCIU/AEI/10.13039/501100011033 and EU.
Generative AI tools (e.g., ChatGPT) were used solely for language editing, improving readability, coding support (syntax and debugging), and assistance in generating plots. The authors take full responsibility for the content of the manuscript.

References

Andreas, E. L.: A theory for the scalar roughness and the scalar transfer coefficients over snow and sea ice, Boundary Layer Meteorol., 38, 159–184, https://doi.org/10.1007/BF00121562, 1987.

Andreas, E. L., Persson, P. O. G., Grachev, A. A., Jordan, R. E., Horst, T. W., Guest, P. S., and Fairall, C. W.: Parameterizing turbulent exchange over sea ice in winter, J. Hydrometeorol., 11, 87–104, https://doi.org/10.1175/2009JHM1102.1, 2010.

Barella, R., Bavay, M., Carletti, F., Mazza, A., Scheidt, K. T., Walter, B., and Marin, C.: Characterizing Snow Roughness: A Novel Low-Cost Portable Tool Based on Charuco Board and Digital Photography, Cold Regions Science and Technology, p. 105013, https://doi.org/10.1016/j.coldregions.2026.105013, 2026.

Barnett, T. P., Adam, J. C., and Lettenmaier, D. P.: Potential impacts of a warming climate on water availability in snow-dominated regions, Nature, 438, 303–309, https://doi.org/10.1038/nature04141, 2005.

Bartelt, P. and Lehning, M.: A physical SNOWPACK model for the Swiss avalanche warning: Part I: numerical model, Cold Reg. Sci. Technol., 35, 123–145, https://doi.org/10.1016/S0165-232X(02)00074-5, 2002.

Beljaars, A. and Holtslag, A.: Flux parameterization over land surfaces for atmospheric models, J. Appl. Meteorol. Climatol., 30, 327–341, https://doi.org/10.1175/1520-0450(1991)030<0327:FPOLSF>2.0.CO;2, 1991.

Beniston, M., Farinotti, D., Stoffel, M., Andreassen, L. M., Coppola, E., Eckert, N., Fantini, A., Giacona, F., Hauck, C., Huss, M., et al.: The European mountain cryosphere: a review of its current state, trends, and future challenges, Cryosphere, 12, 759–794, https://doi.org/10.5194/tc-12-759-2018, 2018.

Braithwaite, R. J.: Aerodynamic stability and turbulent sensible-heat flux over a melting ice surface, the Greenland ice sheet, J. Glaciol., 41, 562–571, https://doi.org/10.3189/S0022143000034882, 1995.

Braithwaite, R. J. and Olesen, O. B.: Response of the energy balance on the margin of the Greenland ice sheet to temperature changes, J. Glaciol., 36, 217–221, https://doi.org/10.3189/S0022143000009461, 1990.

Brock, B. W., Willis, I. C., and Sharp, M. J.: Measurement and parameterization of aerodynamic roughness length variations at Haut Glacier d'Arolla, Switzerland, J. Glaciol., 52, 281–297, https://doi.org/10.3189/172756506781828746, 2006.

Buchmann, N., Hortnagl, L., Keller, S., and Kohonen, K.-M.: Fluxnet Archive Product from Alp Weissenstein, 2006–2023, https://hdl.handle.net/11676/YTVB92-LRk51MUP_JShi7f4u, 2024.

Buri, P., Fatichi, S., Shaw, T. E., Miles, E. S., McCarthy, M. J., Fyffe, C. L., Fugger, S., Ren, S., Kneib, M., Jouberton, A., et al.: Land Surface Modeling in the Himalayas: On the Importance of Evaporative Fluxes for the Water Balance of a High-Elevation Catchment, J. Water Resour. Res., 59(10), e2022WR033 841, https://doi.org/10.1029/2022WR033841, 2023.

Calanca, P.: A note on the roughness length for temperature over melting snow and ice, Q. J. R. Meteorolog. Soc., 127, 255–260, https://doi.org/10.1002/qj.49712757114, 2001.

Centre, E. T., Buchmann, N., Eugster, W., Fuchs, K., and Hortnagl, L.: Fluxnet Product from Früebüel, 2004-12-31–2018-12-31, https://hdl.handle.net/11676/XKMEW1hluNR-eiHFS8ExRnOK, 2019.

Chambers, J. R., Smith, M. W., Smith, T., Sailer, R., Quincey, D. J., Carrivick, J. L., Nicholson, L., Mertes, J., Stiperski, I., and James, M. R.: Correcting for systematic underestimation of topographic glacier aerodynamic roughness values from Hintereisferner, Austria, Front. Earth Sci., 9, 691 195, https://doi.org/10.3389/feart.2021.691195, 2021.

Cremonese, E., Galvagno, M., and Morra di Cella, U.: Fluxnet Archive Product, Torgnon, 2016–2023, https://hdl.handle.net/11676/T2KUGCEIQbE_2ON5kLLORnud, 2024.

https://doi.org/10.5194/egusphere-2026-3417
Preprint. Discussion started: 29 July 2026

Denby, B. and Greuell, W.: The use of bulk and profile methods for determining surface heat fluxes in the presence of glacier winds, J. Glaciol., 46, 445–452, https://doi.org/10.3189/172756500781833124, 2000.

Dozier, J. and Warren, S. G.: Effect of viewing angle on the infrared brightness temperature of snow, Water Resour. Res., 18, 1424–1434, https://doi.org/10.1029/WR018i005p01424, 1982.

Dyer, A. and Hicks, B.: Flux-gradient relationships in the constant flux layer, Q. J. R. Meteorolog. Soc., 96, 715–721, https://doi.org/10.1002/qj.49709641012, 1970.

Dyer, A. and Hicks, B.: The spatial variability of eddy fluxes in the constant flux layer, Q. J. R. Meteorolog. Soc., 98, 206–212, https://doi.org/10.1002/qj.49709841518, 1972.

Esri: World Imagery, ArcGIS Online basemap, https://www.arcgis.com/home/item.html?id=10df2279f9684e4a9f6a7f08febac2a9, accessed 2026-06-15. Sources: Esri, Vantor, Earthstar Geographics, and the GIS User Community., 2026.

Essery, R.: A factorial snowpack model (FSM 1.0), Geosci. Model Dev., 8, 3867–3876, https://doi.org/10.5194/gmd-8-3867-2015, 2015.

Fassnacht, S. R.: Temporal changes in small scale snowpack surface roughness length for sublimation estimates in hydrological modelling, Cuad. Invest. Geog., pp. 43–58, 2010.

Fassnacht, S. R., Stednick, J., Deems, J., and Corrao, M.: Metrics for assessing snow surface roughness from digital imagery, Water Resour. Res., 45(4), https://doi.org/10.1029/2008WR006986, 2009a.

Fassnacht, S. R., Williams, M., and Corrao, M.: Changes in the surface roughness of snow from millimetre to metre scales, Ecol. Complex., 6(3), 221–229, https://doi.org/10.1016/j.ecocom.2009.05.003, 2009b.

Fassnacht, S. R., Suzuki, K., Sanow, J. E., Sexstone, G. A., Pfohl, A. K., Tedesche, M. E., Simms, B. M., and Thomas, E. S.: Snow surface roughness across spatio-temporal scales, Water, 15, 2196, https://doi.org/10.3390/w15122196, 2023.

Fitzpatrick, N., Radić, V., and Menounos, B.: Surface energy balance closure and turbulent flux parameterization on a mid-latitude mountain glacier, Purcell Mountains, Canada, Front. Earth Sci., 5, 67, https://doi.org/10.3389/feart.2017.00067, 2017.

Fitzpatrick, N., Radić, V., and Menounos, B.: A multi-season investigation of glacier surface roughness lengths through in situ and remote observation, Cryosphere, 13, 1051–1071, https://doi.org/10.5194/tc-13-1051-2019, 2019.

Gianelle, D., Belelli Marchesini, L., Marcolla, B., Sottocornola, M., and ICOS Ecosystem Thematic Centre: Warm winter 2020 ecosystem eddy covariance flux product from Monte Bondone, https://doi.org/10.18160/G9KE-399C, 2022.

Gianelle, D., Belelli Marchesini, L., Cavagna, M., Marcolla, B., Rodeghiero, M., Vescovo, L., and Zampedri, R.: ETC L2 ARCHIVE, Monte Bondone, 2022-01-01–2024-10-21, https://hdl.handle.net/11676/PWUVtBkxXOWvni4_qzVlv695, 2024.

Grachev, A. A., Leo, L. S., Sabatino, S. D., Fernando, H. J., Pardyjak, E. R., and Fairall, C. W.: Structure of turbulence in katabatic flows below and above the wind-speed maximum, Boundary Layer Meteorol., 159, 469–494, https://doi.org/10.1007/s10546-015-0034-8, 2016.

Guo, S., Chen, R., Han, C., Liu, J., Wang, X., and Liu, G.: Five-Year Analysis of Evaposublimation Characteristics and Its Role on Surface Energy Balance SEB on a Midlatitude Continental Glacier, Earth Space Sci., 8, 1–16, https://doi.org/10.1029/2021EA001901, 2021.

Hanich, L., Lahnik, O., Gascoin, S., Chakir, A., and Simonneaux, V.: Quantifying snow sublimation by Eddy covariance measurements on the High Atlas Mountain of Marrakech at Tazaghart plateau, Morocco, vol. 385, pp. 387–391, Proc. Int. Assoc. Hydrol. Sci., https://doi.org/10.5194/piahs-385-387-2024, 2024.

Hay, J. and Fitzharris, B.: A comparison of the energy-balance and bulk-aerodynamic approaches for estimating glacier melt, J. Glaciol., 34, 145–153, https://doi.org/10.3189/S0022143000032172, 1988.

Herrero, J. and Polo, M. J.: Evaposublimation from the snow in the Mediterranean mountains of Sierra Nevada (Spain), Cryosphere, 10(6), 2981–2998, https://doi.org/10.5194/tc-10-2981-2016, 2016.

https://doi.org/10.5194/egusphere-2026-3417
Preprint. Discussion started: 29 July 2026

Herrero, J., Polo, M., Moñino, A., and Losada, M.: An energy balance snowmelt model in a Mediterranean site, J. Hydrol., 371, 98–107, https://doi.org/10.1016/j.jhydrol.2009.03.021, 2009.

Heusinkveld, B. G., Jacobs, A. F., and Holtslag, A. A.: Effect of open-path gas analyzer wetness on eddy covariance flux measurements: A proposed solution, Agric. For. Meteorol., 148, 1563–1573, https://doi.org/10.1016/j.agrformet.2008.05.010, 2008.

Hock, R.: Glacier melt: a review of processes and their modelling, Prog. Phys. Geogr., 29, 362–391, https://doi.org/10.1191/0309133305pp453ra, 2005.

Hock, R. and Holmgren, B.: A distributed surface energy-balance model for complex topography and its application to Storglaciären, Sweden, J. Glaciol., 51, 25–36, https://doi.org/10.3189/172756505781829566, 2005.

Hoffman, M. J., Fountain, A. G., and Liston, G. E.: Surface energy balance and melt thresholds over 11 years at Taylor Glacier, Antarctica, J. Geophys. Res.: Earth Surf., 113, https://doi.org/10.1029/2008JF001029, 2008.

Hood, E., Williams, M., and Cline, D.: Sublimation from a seasonal snowpack at a continental, mid-latitude alpine site, Hydrol. Process., 13, 1781–1797, https://doi.org/10.1002/(SICI)1099-1085(199909)13:12/13<1781::AID-HYP860>3.0.CO;2-C, 1999.

Kljun, N., Calanca, P., Rotach, M. W., and Schmid, H. P.: A simple two-dimensional parameterisation for Flux Footprint Prediction (FFP), Geosci. Model Dev., 8, 3695–3713, https://doi.org/10.5194/gmd-8-3695-2015, 2015.

Lehner, M., Rotach, M. W., Sfyri, E., and Obleitner, F.: Spatial and temporal variations in near-surface energy fluxes in an alpine valley under synoptically undisturbed and clear-sky conditions, Q. J. R. Meteorolog. Soc., 147, 2173–2196, https://doi.org/10.1002/qj.4016, 2021.

Lehning, M., Bartelt, P., Brown, B., Russi, T., Stöckli, U., and Zimmerli, M.: SNOWPACK model calculations for avalanche warning based upon a new network of weather and snow stations, Cold Reg. Sci. Technol., 30, 145–157, https://doi.org/10.1016/S0165-232X(99)00022-1, 1999.

Lehning, M., Bartelt, P., Brown, B., Fierz, C., and Satyawali, P.: A physical SNOWPACK model for the Swiss avalanche warning: Part II. Snow microstructure, Cold Reg. Sci. Technol., 35, 147–167, https://doi.org/10.1016/S0165-232X(02)00073-3, 2002.

Lettau, H.: Note on aerodynamic roughness-parameter estimation on the basis of roughness-element description, J. Appl. Meteorol. (1962-1982), 8, 828–832, 1969.

Li, L. and Pomeroy, J. W.: Probability of occurrence of blowing snow, J. Geophys. Res.: Atmos., 102, 21 955–21 964, https://doi.org/10.1029/97JD01522, 1997.

Litt, M., Sicart, J.-E., and Helgason, W.: A study of turbulent fluxes and their measurement errors for different wind regimes over the tropical Zongo Glacier (16° S) during the dry season, Atmos. Meas. Tech., 8, 3229–3250, https://doi.org/10.5194/amt-8-3229-2015, 2015.

Liu, J., Chen, R., Ma, S., Guo, S., Han, C., and Ding, Y.: Quantifying the Aerodynamic Roughness Length of Snow Surfaces With Time-Lapse Structure-From-Motion, J. Geophys. Res. D: Atmos., 128(3), e2022JD037 032, https://doi.org/10.1029/2022JD037032, 2023.

Lundquist, J. D., Vano, J., Gutmann, E., Hogan, D., Schwat, E., Haugeneder, M., Mateo, E., Oncley, S., Roden, C., Osenga, E., et al.: Sublimation of Snow, Bull. Am. Meteorol. Soc., 105, E975–E990, https://doi.org/10.1175/BAMS-D-23-0191.1, 2024.

Mahrt, L.: Stably stratified atmospheric boundary layers, Annu. Rev. Fluid Mech., 46, 23–45, https://doi.org/10.1146/annurev-fluid-010313-141354, 2014.

Martin, E. and Lejeune, Y.: Turbulent fluxes above the snow surface, Ann. Glaciol., 26, 179–183, https://doi.org/10.3189/1998AoG26-1-179-183, 1998.

Munro, D. S.: Surface roughness and bulk heat transfer on a glacier: comparison with eddy correlation, J. Glaciol., 35, 343–348, https://doi.org/10.3189/S0022143000009266, 1989.

https://doi.org/10.5194/egusphere-2026-3417
Preprint. Discussion started: 29 July 2026

Pastorello, G., Trotta, C., Canfora, E., Chu, H., Christianson, D., Cheah, Y.-W., Poindexter, C., Chen, J., Elbashandy, A., Humphrey, M., et al.: The FLUXNET2015 dataset and the ONEFlux processing pipeline for eddy covariance data, Sci. Data, 7, 225, https://doi.org/10.6084/m9.figshare.12295910, 2020.

Radić, V., Menounos, B., Shea, J., Fitzpatrick, N., Tessema, M. A., and Déry, S. J.: Evaluation of different methods to model near-surface turbulent fluxes for a mountain glacier in the Cariboo Mountains, BC, Canada, Cryosphere, 11, 2897–2918, https://doi.org/10.5194/tc-11-2897-2017, 2017.

Rotach, M. W., Stiperski, I., Fuhrer, O., Goger, B., Gohm, A., Obleitner, F., Rau, G., Sfyri, E., and Vergeiner, J.: Investigating exchange processes over complex topography: The Innsbruck box (i-Box), Bull. Am. Meteorol. Soc., 98, 787–805, https://doi.org/10.1175/BAMS-D-15-00246.1, 2017.

Scheidt, K. T., Pimentel, R., Premier, V., Marin, C., Polo, M. J., and Notarnicola, C.: Assessing the impact of terrestrial photography-derived roughness lengths on evaposublimation from seasonal snow in the Mediterranean mountains of Sierra Nevada (Spain), J. Hydrol.: Reg. Stud., 60, 102 431, https://doi.org/10.1016/j.ejrh.2025.102431, 2025.

Schlögl, S., Lehning, M., and Mott, R.: How are turbulent sensible heat fluxes and snow melt rates affected by a changing snow cover fraction?, Front. Earth Sci., 6, 154, https://doi.org/10.3389/feart.2018.00154, 2018.

Sfyri, E., Rotach, M. W., Stiperski, I., Bosveld, F. C., Lehner, M., and Obleitner, F.: Scalar-flux similarity in the layer near the surface over mountainous terrain, Boundary Layer Meteorol., 169, 11–46, https://doi.org/10.1007/s10546-018-0365-3, 2018.

Sicart, J. E., Wagnon, P., and Ribstein, P.: Atmospheric controls of the heat balance of Zongo Glacier (16 S, Bolivia), J. Geophys. Res.: Atmos., 110, https://doi.org/10.1029/2004JD005732, 2005.

Sigmund, A., Dujardin, J., Comola, F., Sharma, V., Huwald, H., Melo, D. B., Hirasawa, N., Nishimura, K., and Lehning, M.: Evidence of strong flux underestimation by bulk parametrizations during drifting and blowing snow, Boundary Layer Meteorol., 182, 119–146, https://doi.org/10.1007/s10546-023-00809-x, 2022.

Smeets, C. and Van den Broeke, M.: The parameterisation of scalar transfer over rough ice, Boundary Layer Meteorol., 128, 339–355, https://doi.org/10.1007/s10546-008-9292-z, 2008.

Smith, M. W., Quincey, D. J., Dixon, T., Bingham, R. G., Carrivick, J. L., Irvine-Fynn, T. D., and Rippin, D. M.: Aerodynamic roughness of glacial ice surfaces derived from high-resolution topographic data, J. Geophys. Res. F: Earth Surf., 121, 748–766, https://doi.org/10.1002/2015JF003759, 2016.

Stigter, E. E., Litt, M., Steiner, J. F., Bonekamp, P. N., Shea, J. M., Bierkens, M. F., and Immerzeel, W. W.: The importance of snow sublimation on a Himalayan glacier, Front. Earth Sci., 6, 108, https://doi.org/10.3389/feart.2018.00108, 2018.

Stiperski, I. and Rotach, M. W.: On the measurement of turbulence over complex mountainous terrain, Boundary Layer Meteorol., 159, 97–121, https://doi.org/10.1007/s10546-015-0103-z, 2016.

Strasser, U., Bernhardt, M., Weber, M., Liston, G., and Mauser, W.: Is snow sublimation important in the alpine water balance?, Cryosphere, 2, 53–66, https://doi.org/10.5194/tc-2-53-2008, 2008.

Strasser, U., Warscher, M., Rottler, E., and Hanzer, F.: openAMUNDSEN v1. 0: an open-source snow-hydrological model for mountain regions, Geosci. Model Dev., 17, 6775–6797, https://doi.org/10.5194/gmd-17-6775-2024, 2024.

Stull, R. B.: Similarity Theory, in: An Introduction to Boundary Layer Meteorology, pp. 347–404, Springer, 1988.

University of Innsbruck, ACInn: Weather Station Portal, https://acinn-data.uibk.ac.at/pages/station-list.html, accessed: 01 August 2025, n.d.

Vano, J. A., Udall, B., Cayan, D. R., Overpeck, J. T., Brekke, L. D., Das, T., Hartmann, H. C., Hidalgo, H. G., Hoerling, M., McCabe, G. J., et al.: Understanding uncertainties in future Colorado River streamflow, Bull. Am. Meteorol. Soc., 95, 59–78, https://doi.org/10.1175/BAMS-D-12-00228.1, 2014.

Voisin, D., Biron, R., Cohard, J.-M., Coulaud, C., Foret, J., Foulquier, A., Liger, L., Salze, P., and Valay, J.-G.: ETC L2 ARCHIVE, Col du Lautaret, 2021-12-31–2023-12-31, https://hdl.handle.net/11676/3_f7_9QXtKOQikwW6cmTkRvi, 2024.

Volk, J. M., Huntington, J., Melton, F. S., Allen, R., Anderson, M. C., Fisher, J. B., Kilic, A., Senay, G., Halverson, G., Knipper, K., et al.: Development of a benchmark eddy flux evapotranspiration dataset for evaluation of satellite-driven evapotranspiration models over the CONUS, Agric. For. Meteorol., 331, 109 307, https://doi.org/10.1016/j.agrformet.2023.109307, 2023.

Von Kármán, T.: Mechanical similitude and turbulence, 611, National Advisory Committee for Aeronautics, 1931.

Voordendag, A., Réveillet, M., MacDonell, S., and Lhermitte, S.: Snow model comparison to simulate snow depth evolution and sublimation at point scale in the semi-arid Andes of Chile, Cryosphere, 15, 4241–4259, https://doi.org/10.5194/tc-15-4241-2021, 2021.

Wohlfahrt, G.: Fluxnet Product from Neustift, 2001-12-31–2020-12-31, https://hdl.handle.net/11676/SJV9f8yU8TsFZH4aZfXgkVpc, 2024.

Wohlfahrt, G. and Niedrist, G.: IT-MtP Muntatschinig Pasture – European Fluxes Database Cluster, https://www.europe-fluxdata.eu/home/site-details?id=IT-MtP, site-level eddy covariance data. Accessed: 15 January 2026, n.d.